Lithos 202–203 (2014) 1–20

Contents lists available at ScienceDirect

Lithos

journal homepage: www.elsevier.com/locate/lithos

# Geochemical and geochronologic constraints for Paleozoic magmatism related to the orogenic collapse in the Qimantagh–South Altyn region, northwestern China

Chao Wang [a,*], Liang Liu [b], Pei-Xi Xiao [a], Yu-Ting Cao [c], Hui-Yang Yu [a], Joseph G. Meert [d], Wen-Tian Liang [b]

[a] MLR Key Laboratory of Genesis and Exploration of Magmatic Ore Deposits, Orogen Research Centre of China Geological Survey, Xi'an Center of Geological Survey, Xi'an 710054, China
[b] State Key Laboratory of Continental Dynamics, Department of Geology, Northwest University, Xi'an 710069, China
[c] College of Geological Science & Engineering, Shandong University of Science and Technology, Qingdao 266510, China
[d] Department of Geological Sciences, University of Florida, 241 Williamson Hall, Gainesville, FL 32611, USA

ARTICLE INFO

*Article history:*
Received 3 February 2014
Accepted 18 May 2014
Available online 25 May 2014

*Keywords:*
Post-collisional
Orogenic collapse
Granites
Altyn Tagh
East Kunlun

ABSTRACT

Voluminous and discrete early Paleozoic bimodal magmatic suites are thought to be the result of post-collisional extension following the amalgamation of East Kunlun and Altyn Tagh. In this paper, four representative magmatic units were studied for their geochemical fingerprint in conjunction with geochronological studies. The 467–445 Ma Mangya mafic suite shows E-MORB type rare earth element (REE) patterns that are the result of asthenospheric interaction with a metasomatized subcontinental lithosphere. High-K calc-alkaline granodiorites, intruded at ca. 450 Ma, are characterized by high Mg#, the least fractionated REE pattern without an Eu anomaly, as well as high Sr and low Rb/Sr ratio. We interpret these geochemical signals to result from lower crustal melting of garnet amphibolite at pressures between 16 and 22 kbar. A 430–420 Ma A-type granite is interpreted to result from the melting of metaigneous rocks at middle to lower crustal depths. Lastly, a late magmatic pulse occurs between 400 and 380 Ma and is represented by the Alk granite. The Alk granite is interpreted to be a product of metapelite melts and is associated with a smaller volume of mafic melts. U–Pb zircon geochronology of Paleozoic igneous rocks of the Qimantagh–South Altyn reveals that most of the magmatic episodes are either coeval with, or post, extensional deformation. This phase of extension is supported by the exhumation of HP/UHP metamorphic rocks and crustal anatexis. Collectively, the evolutionary stages documented in this study correspond to a succession of post-collisional, postorogenic and, ultimately, within plate magmatic episodes. The overall features support orogenic collapse via removal of a thickened lithospheric root beneath the East Kunlun–Altyn Tagh collisional orogen during early Paleozoic.



## 1. Introduction

Large orogenic belts formed at convergent plate boundaries comprise a period of continent–continent or arc–continent collision accommodated by crustal thickening (Dewey and Bird, 1970). The crustal thickening is followed by syn- to post-convergence extension and thinning of that previously thickened crust (e.g. Coney and Harms, 1984; Dewey, 1988; England, 1993; Platt and Vissers, 1989; Vanderhaeghe and Teyssier, 2001). Extension and crustal thinning of previously thickened crust following collision are sometimes referred to as 'relaxation phases' (Liégeois, 1998). These post-collisional (either late or postorogenic) settings are normally accompanied by voluminous, mostly granitoid magmatism, contain varying quantities of mafic microgranular enclaves or coeval mafic magmatism (bi-modal suites; e.g. Bonin, 2004; Liégeois et al., 1998; Turner, 1992; Turner et al., 1999). Magmatism often displays an evolutionary progression from high-K calc-alkaline (I-type) to alkaline (A-type) compositions, representing the magmatism in post-collisional and postorogenic settings and the transition from crustal thickening to the onset of crustal thinning associated with orogenic collapse (e.g. Bonin, 2004; Clemens et al., 2009; Liégeois et al., 1998; Oyhantçabal et al., 2007; Wang et al., 2007).

Northeastern Tibet is an early Paleozoic orogenic collage exposed in the Altyn Tagh, East Kunlun, North Qadidam, and Qilian Shan regions (Fig. 1a; Che et al., 1995; Jiang et al., 1992; Sobel and Arnaud, 1999; Xu et al., 2007; Yin and Harrison, 2000). Within each of these regions there are abundant early Paleozoic HP/UHP metamorphic rocks along with mafic–ultramafic and granitic magmatism. The Altyn Tagh and East Kunlun are the two major orogenic belts in this collage (Fig. 1b). The Altyn Tagh fault separates the Altyn Tagh region in the north from the East Kunlun region in the south (Fig. 1b). Although both regions are the foci of numerous studies, the details of the Paleozoic evolutionary relationships between these two regions are scarce. In the southern

* Corresponding author. Tel.: +86 29 87821741; fax: +86 29 88304789.
*E-mail address:* wangc-mail@163.com (C. Wang).

http://dx.doi.org/10.1016/j.lithos.2014.05.016
0024-4937/

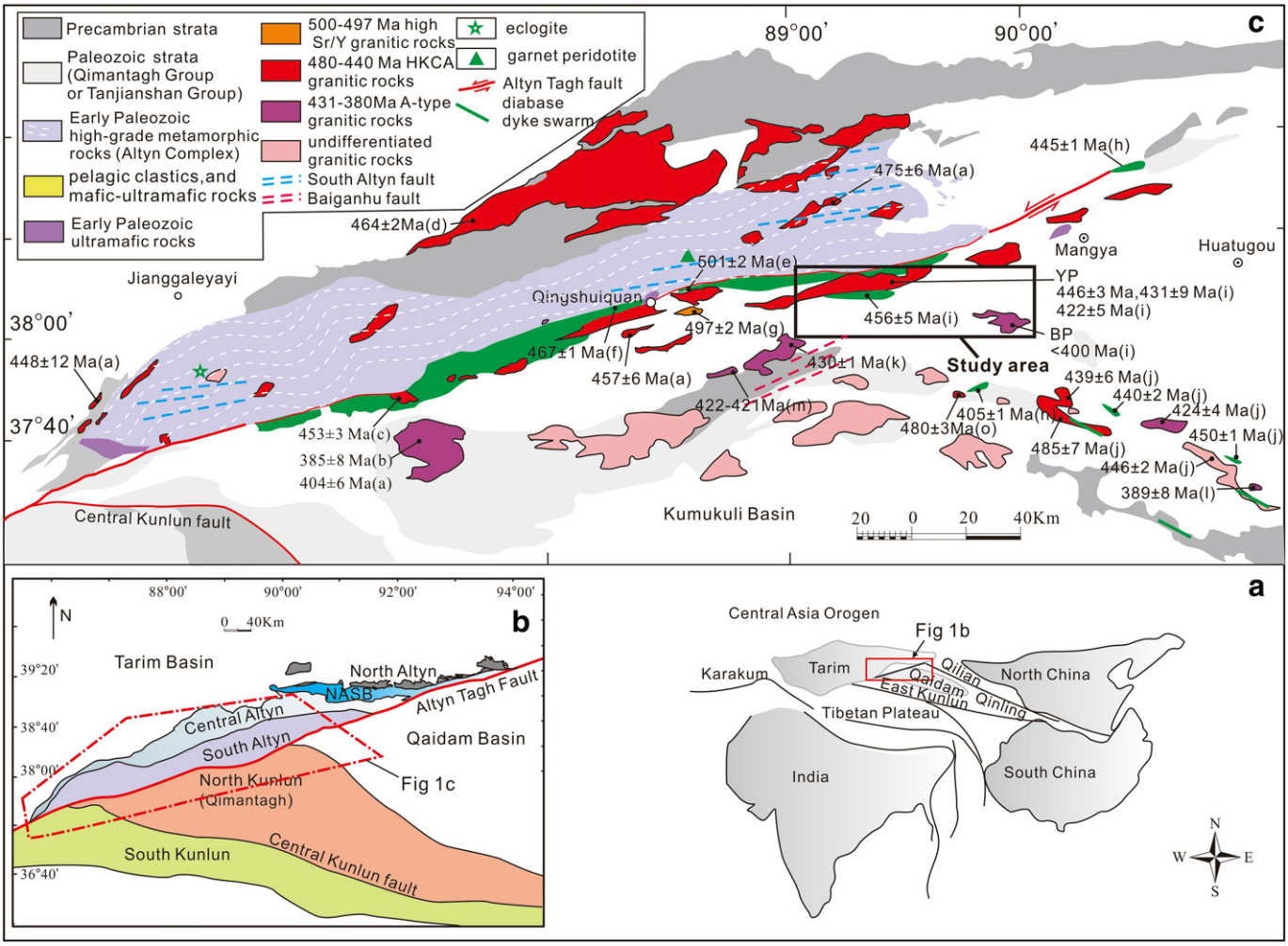


**Fig. 1.** (a) Location of Altyn Tagh and adjoining regions. (b) Schematic distribution of main geotectonic units in the Altyn Tagh and East Kunlun: North Altyn Tagh Archean terrain (North Altyn) and North Altyn Tagh subduction–collision belt (NASB) in the north, the Central Altyn massif (CAM) in the middle, and the South Altyn Tagh subduction–collision belt (South Altyn) in the southwest. (c) Sketch geological map of Altyn Tagh (after Wang et al., 2013). Black rectangle indicates location of the study area. U–Pb ages for early Paleozoic magmatic rocks are indicated in the map. Data sources are superscripted as follows: (a) Cowgill et al. (2003); (b) Wu et al. (2007); (c) Yang et al. (2012); (d) Cao et al. (2010); (e) Li et al. (2009); (f) Ma et al. (2011); (g) Sun et al. (2012); (h) Dong et al. (2011); (i) this study; (j) Li et al. (2013); (k) Gao and Li (2011); (l) Guo et al. (2011); (m) Li et al. (2012); (n) Wang et al. (2010); (o) Cui et al. (2011). HKCA—high-K calc-alkaline.
The South Altyn faults are after Cui (2011); the Baiganhu faults are after Feng et al. (2013); the diabase dyke swarms are after Qi et al. (2013).

Altyn belt high-pressure and ultra-high pressure (HP/UHP) metamorphic rocks are juxtaposed and represent an episode of continent–continent collision around 500 Ma (Liu et al., 2012 and references therein). Recently, abundant Paleozoic magmatic assemblages, located along the southern margin of the Altyn Tagh (South Altyn) and the northwest part of East Kunlun (Qimantagh), were reported (e.g. Gao and Li, 2011; Guo et al., 2011; Li et al., 2013; Ma et al., 2011; Wang et al., 2008). Liu et al. (2013) suggested that the 466–385 Ma granitoid intrusions occur in conjunction with the exhumation of the southern Altyn HP/UHP rocks and associated slab breakoff of subducted continental and oceanic crust. As a part of our systematic investigation of granitoids in these areas, we found that the magmatism in the Qimantagh region is coeval with magmatism in the South Altyn area. The majority of these intrusions are high-K calc-alkaline or alkaline granitoids with associated mafic–ultramafic rocks. We make the argument that the magmatic activity in these two regions reflects the transition from crustal thickening associated with final collision and the onset of extensional collapse of the orogen. Thus, a better understanding of the genetic relationships between the various magmatic bodies can be used to provide a framework for the geological evolution of the East Kunlun and Altyn Tagh regions.

In this paper, the main objectives are (1) to report geochemical and U–Pb geochronological data from Ordovician–Devonian mafic and granitic rocks from northern margin of the Qimantagh that display the distinctive chemical features in magma source regions; (2) to describe and interpret the spatial–temporal links between post-collisional and post-orogenic magmatism within the Qimantagh and South Altyn areas; and (3) to integrate these studies with the structural and metamorphic history of the Qimantagh and South Altyn in order to constrain geodynamic models of late orogenesis and extensional collapse.

## 2. Geological setting

The East Kunlun encompasses both the North Kunlun terrane and the South Kunlun terrane (Fig. 1b; Bian et al., 2004; Li et al., 2006; Wu et al., 1989; Xu et al., 2006). The East Kunlun consists of Paleo- and Mesoproterozoic and early Paleozoic strata covered by late Devonian-aged red molasse deposits. The Central Kunlun fault zone marks a major suture zone representing the boundary between the North Kunlun and South Kunlun terranes (Pan et al., 1996; Wu et al., 1989; Xu et al., 2006). The western part of North Kunlun terrane that borders the South Altyn region is known as the Qimantagh area. The basement

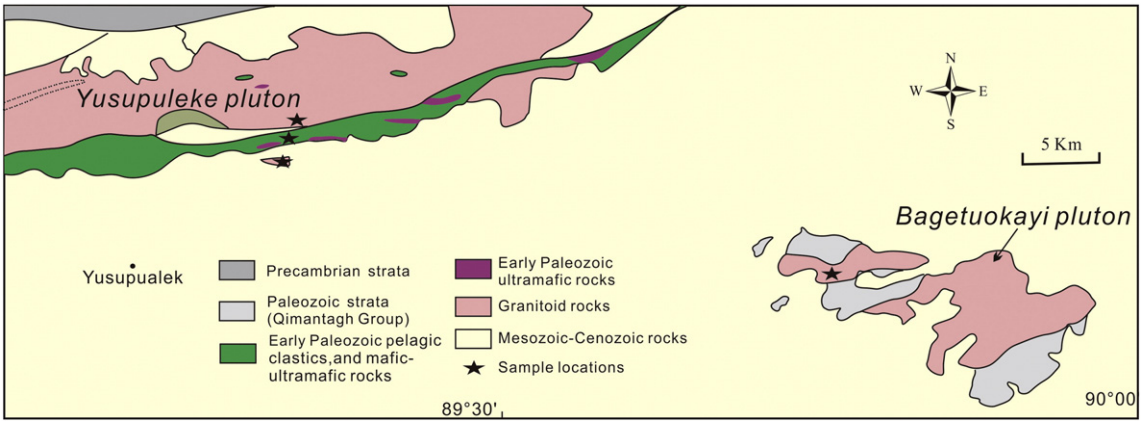


**Fig. 2.** Geological map of the study area in southern sector of the South Altyn (modified after XACGS, 2003). Locations of analyzed samples used in this study are shown.

of the Qimantagh area includes the Neoarchean to Mesoproterozoic Jinshuikou Group and the Neoproterozoic Binggou Group. The Ordovician–Silurian Qimantagh Group or Tanjianshan Group is widely distributed in the region and includes shallow and deep-water clastics, carbonates, volcanic rocks and volcaniclastic rocks, formed in an extensional setting (Jiang et al., 1992; Wang et al., 2010, 2012). Late Paleozoic strata overlay these sequences. Late Devonian strata contain both clastic and terrestrial volcanic rocks that represent molasse deposition marking the end of an early Paleozoic orogeny (Cui et al., 2011; Jiang et al., 1992; Lu et al., 2010).

The Altyn Tagh is subdivided into four units. From north to south these are referred to as the North Altyn Tagh Archean terrain (North Altyn), the North Altyn Tagh early Paleozoic subduction–collision belt (NASB), the Central Altyn massif (CAM), and the South Altyn Tagh subduction–collision belt (South Altyn) based on their stratigraphy, metamorphic grade, structure and ages (Fig. 1b; Liu et al., 2009). The South Altyn consists mainly of early Paleozoic HP/UHP metamorphic rocks, mafic–ultramafic rocks, granites and minor clastics. The vast high-grade metamorphic rocks from the South Altyn were named the "Altyn Complex" (Wang et al., 2013). New data suggest that the protolith of the Altyn Complex was part of the Neoproterozoic southeastern margin of the Tarim craton (Wang et al., 2013). The HP/UHP metamorphic rocks in the South Altyn include garnet-bearing pelitic gneisses, eclogite, kyanite + garnet gneisses, magnesite-bearing garnet peridotite, granitic gneiss, and K-feldspar bearing garnet clinopyroxenite (e.g. Cao et al., 2009; Liu et al., 1996, 2002, 2004, 2005, 2007, 2012; Wang et al., 2011; Zhang et al., 2001, 2002, 2005). These HP/UHP metamorphic rocks have metamorphic ages between 510 and 450 Ma (Cao et al., 2009, 2013; Liu et al., 2009, 2012; Wang et al., 2011, 2013; Zhang et al., 1999, 2004, 2005). Geochronological data demonstrate that peak eclogite-facies metamorphic conditions existed in the South Altyn at ca. 510–500 Ma (Liu et al., 2009, 2012; Wang et al., 2011; Zhang et al., 2005). Retrograde HP granulite-facies rocks developed around 454 Ma (Liu et al., 2012). The foliation-parallel leucosome in the South Altyn is from a migmatitic environment

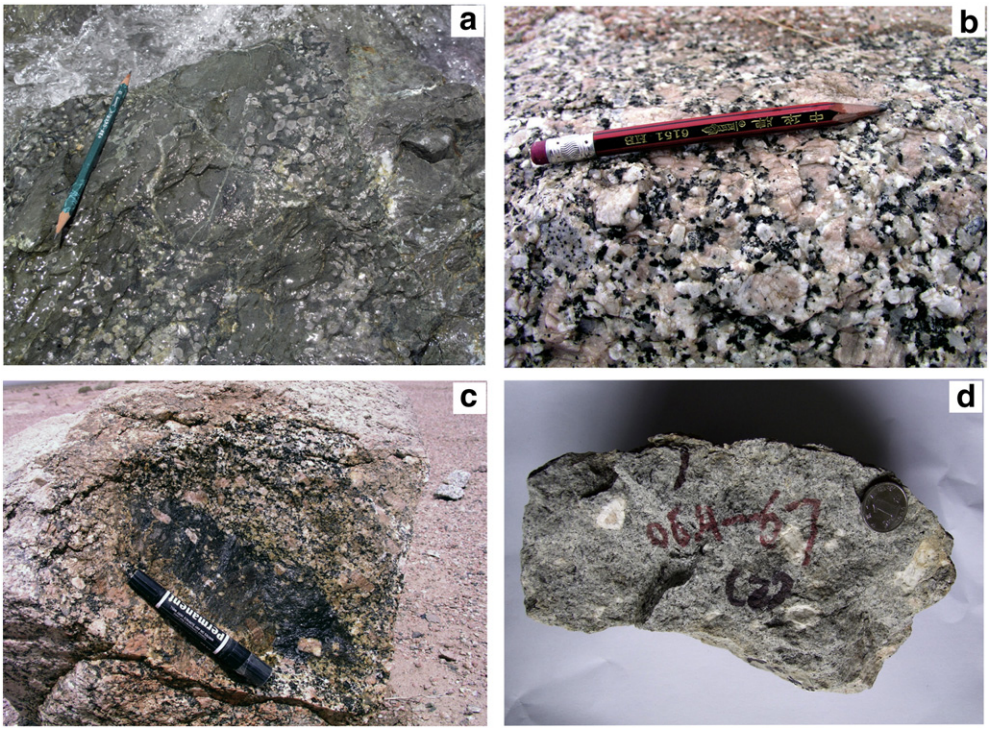


**Fig. 3.** (a) Fine-grained, amygdaloidal mafic lava from the South Altyn. (b) Monzogranite from YP displays rapakivi textures, characterized by the occurrence of plagioclase-mantled K-feldspar phenocrysts. (c) Some elongated enclaves define a distinct magmatic foliation in the monzogranite from YP. (d) Feldspar phenocrysts showing rapakivi texture from the aplitic dykes of YP.

**Table 1**
Major- and trace-element analytical data.

| Area | Mangya mafic rocks | | | | | | Yusupuleke pluton | | | | | | | |
|---|---|---|---|---|---|---|---|---|---|---|---|---|---|---|
| Rock-type | Diabase | | | | | Basalt | Granodiorite | | | | Monzogranite | | | |
| Sample | 10A-06/7 | 10A-06/9 | 10A-06/10 | 10A-06/8 | 10A-06/11 | 10A-06/1 | 10A-06/12 | 10A-06/13 | 10A-06/15 | 10A-06/16 | 06A-60 | 06A-61 | 06A-63 | 06A-64 |
| $SiO_2$ | 48.3 | 48.7 | 49.4 | 49.1 | 50.4 | 47.0 | 68.4 | 66.3 | 61.7 | 71.3 | 67.8 | 67.8 | 68.9 | 63.5 |
| $TiO_2$ | 1.25 | 1.33 | 1.33 | 2.66 | 1.89 | 2.06 | 0.43 | 0.51 | 0.71 | 0.31 | 0.63 | 0.65 | 0.57 | 0.89 |
| $Al_2O_3$ | 14.9 | 13.6 | 15.4 | 13.1 | 13.3 | 12.9 | 15.0 | 15.4 | 16.0 | 14.5 | 14.7 | 14.5 | 14.6 | 15.5 |
| $TFe_2O_3$ | 10.65 | 9.84 | 10.27 | 14.84 | 13.05 | 14.11 | 3.23 | 3.83 | 6.14 | 2.49 | 3.93 | 3.82 | 3.38 | 5.34 |
| MnO | 0.16 | 0.16 | 0.19 | 0.20 | 0.20 | 0.19 | 0.05 | 0.06 | 0.09 | 0.03 | 0.06 | 0.05 | 0.05 | 0.07 |
| MgO | 8.49 | 7.12 | 7.43 | 5.31 | 6.07 | 7.38 | 1.34 | 1.47 | 2.03 | 0.97 | 1.45 | 1.39 | 1.28 | 2.02 |
| CaO | 7.81 | 10.38 | 9.05 | 8.60 | 9.13 | 10.08 | 3.41 | 3.10 | 5.48 | 2.68 | 2.78 | 2.79 | 2.30 | 3.73 |
| $Na_2O$ | 3.75 | 3.84 | 3.23 | 3.12 | 3.52 | 1.12 | 3.31 | 3.53 | 3.78 | 3.06 | 3.01 | 3.60 | 3.01 | 3.18 |
| $K_2O$ | 0.66 | 0.44 | 1.18 | 0.49 | 0.56 | 1.00 | 3.40 | 3.81 | 2.41 | 3.95 | 4.74 | 4.39 | 5.01 | 4.08 |
| $P_2O_5$ | 0.15 | 0.15 | 0.14 | 0.28 | 0.21 | 0.26 | 0.16 | 0.15 | 0.32 | 0.11 | 0.15 | 0.15 | 0.13 | 0.22 |
| LOI | 3.50 | 4.46 | 2.65 | 2.21 | 2.04 | 3.44 | 0.87 | 1.40 | 0.93 | 0.73 | 1.00 | 0.91 | 0.73 | 1.15 |
| TOTAL | 99.7 | 100.0 | 100.3 | 99.9 | 100.4 | 99.5 | 99.6 | 99.6 | 99.6 | 100.1 | 100.3 | 100.0 | 100.0 | 99.6 |
| Li | 28.8 | 18.1 | 18.9 | 14.3 | 14.2 | 27.0 | 17.8 | 9.4 | 11.4 | 13.9 | - | - | - | - |
| Be | 0.5 | 0.5 | 0.5 | 0.9 | 0.7 | 0.9 | 2.6 | 2.5 | 3.0 | 1.8 | 3.2 | 3.3 | 3.3 | 3.4 |
| Sc | 27.7 | 40.4 | 37.1 | 41.0 | 40.9 | 35.6 | 6.5 | 8.1 | 18.2 | 4.7 | 8.4 | 8.4 | 7.9 | 11.9 |
| V | 216.4 | 259.1 | 263.9 | 419.4 | 334.9 | 325.7 | 46.6 | 53.7 | 106.5 | 34.7 | 48.8 | 48.7 | 42.3 | 73.7 |
| Cr | 164.9 | 155.3 | 393.4 | 11.0 | 23.6 | 245.9 | 20.2 | 23.1 | 29.6 | 16.5 | 23.1 | 18.0 | 15.8 | 26.6 |
| Co | 49.3 | 42.2 | 43.9 | 54.7 | 51.7 | 49.2 | 134.3 | 104.2 | 76.7 | 134.6 | 90.7 | 103.8 | 91.0 | 85.5 |
| Ni | 172.7 | 71.6 | 96.0 | 27.8 | 39.5 | 154.8 | 14.6 | 9.8 | 17.4 | 9.7 | 12.2 | 11.5 | 10.0 | 16.4 |
| Cu | 48.9 | 30.8 | 55.4 | 60.6 | 52.4 | 55.1 | 3.8 | 9.2 | 31.4 | 10.1 | 5.3 | 6.3 | 5.6 | 10.6 |
| Zn | 75.6 | 66.8 | 75.2 | 104.2 | 86.4 | 122.2 | 46.4 | 61.2 | 69.4 | 38.8 | 48.5 | 47.5 | 43.6 | 62.5 |
| Ga | 16.3 | 14.8 | 16.4 | 20.0 | 17.9 | 19.2 | 17.7 | 17.8 | 20.8 | 16.0 | 20.9 | 21.4 | 20.2 | 24.1 |
| Ge | 1.3 | 1.4 | 1.3 | 1.5 | 1.5 | 1.4 | 1.1 | 1.1 | 1.3 | 0.8 | - | - | - | - |
| Rb | 11.3 | 7.4 | 21.1 | 7.5 | 10.7 | 24.4 | 118.6 | 123.4 | 65.2 | 118.2 | 193.7 | 185.1 | 203.8 | 175.3 |
| Sr | 171.1 | 239.4 | 210.0 | 196.8 | 242.1 | 43.7 | 415.3 | 538.5 | 565.1 | 403.1 | 182.8 | 178.1 | 176.5 | 236.2 |
| Y | 26.7 | 30.4 | 28.2 | 49.1 | 38.2 | 46.5 | 16.5 | 14.3 | 29.0 | 7.5 | 43.1 | 44.5 | 51.2 | 40.3 |
| Zr | 90.7 | 91.2 | 91.4 | 173.2 | 130.5 | 163.7 | 178.6 | 174.4 | 206.7 | 136.1 | 212.0 | 288.3 | 272.2 | 355.9 |
| Nb | 6.0 | 5.8 | 5.9 | 11.9 | 8.6 | 10.8 | 13.3 | 13.0 | 21.1 | 6.1 | 19.5 | 20.1 | 20.1 | 22.3 |
| Cs | 0.7 | 0.6 | 1.3 | 1.1 | 1.0 | 1.6 | 2.2 | 1.2 | 1.4 | 2.0 | 6.3 | 6.6 | 6.7 | 5.2 |
| Ba | 179.9 | 112.9 | 374.2 | 139.7 | 167.7 | 60.9 | 792.8 | 737.9 | 843.8 | 1016.2 | 682.2 | 521.0 | 568.3 | 696.3 |
| La | 6.3 | 7.1 | 6.0 | 11.6 | 8.5 | 9.5 | 31.8 | 27.8 | 26.4 | 23.0 | 58.2 | 69.5 | 53.7 | 74.2 |
| Ce | 15.7 | 16.7 | 15.3 | 29.0 | 21.3 | 25.5 | 61.5 | 53.0 | 64.0 | 43.2 | 117.5 | 137.7 | 113.2 | 144.3 |
| Pr | 2.1 | 2.2 | 2.1 | 4.0 | 2.9 | 3.6 | 6.5 | 5.5 | 7.9 | 4.3 | 12.4 | 14.2 | 12.3 | 14.7 |
| Nd | 10.5 | 11.0 | 10.5 | 19.6 | 14.5 | 17.9 | 23.6 | 20.2 | 31.8 | 14.9 | 47.0 | 52.9 | 48.1 | 54.7 |
| Sm | 3.2 | 3.4 | 3.3 | 6.0 | 4.4 | 5.5 | 4.4 | 3.9 | 7.0 | 2.5 | 8.9 | 9.6 | 9.8 | 9.6 |
| Eu | 1.2 | 1.2 | 1.2 | 1.9 | 1.5 | 1.7 | 1.1 | 1.3 | 1.7 | 0.8 | 1.4 | 1.3 | 1.3 | 1.6 |
| Gd | 3.8 | 4.1 | 3.9 | 6.9 | 5.3 | 6.5 | 3.7 | 3.3 | 6.2 | 2.2 | 8.4 | 8.9 | 9.3 | 9.0 |
| Tb | 0.7 | 0.7 | 0.7 | 1.2 | 0.9 | 1.2 | 0.5 | 0.4 | 0.9 | 0.3 | 1.3 | 1.3 | 1.5 | 1.3 |
| Dy | 4.5 | 5.0 | 4.7 | 8.2 | 6.3 | 7.7 | 2.8 | 2.5 | 5.2 | 1.4 | 7.5 | 7.8 | 8.8 | 7.4 |
| Ho | 1.0 | 1.1 | 1.0 | 1.8 | 1.4 | 1.7 | 0.5 | 0.5 | 1.0 | 0.2 | 1.5 | 1.5 | 1.7 | 1.4 |
| Er | 2.7 | 3.2 | 2.9 | 5.1 | 3.9 | 4.8 | 1.5 | 1.3 | 2.7 | 0.7 | 4.2 | 4.3 | 4.9 | 3.9 |
| Tm | 0.4 | 0.5 | 0.4 | 0.8 | 0.6 | 0.7 | 0.2 | 0.2 | 0.4 | 0.1 | 0.6 | 0.7 | 0.8 | 0.6 |
| Yb | 2.6 | 3.0 | 2.7 | 4.8 | 3.7 | 4.5 | 1.4 | 1.3 | 2.5 | 0.6 | 3.7 | 3.9 | 4.4 | 3.6 |
| Lu | 0.4 | 0.5 | 0.4 | 0.7 | 0.5 | 0.7 | 0.2 | 0.2 | 0.4 | 0.1 | 0.6 | 0.6 | 0.6 | 0.5 |
| Hf | 2.3 | 2.4 | 2.4 | 4.4 | 3.3 | 4.2 | 4.3 | 4.1 | 5.0 | 3.5 | 5.4 | 7.1 | 6.7 | 8.7 |
| Ta | 0.4 | 0.4 | 0.4 | 0.8 | 0.5 | 0.7 | 1.2 | 0.9 | 1.4 | 0.5 | 2.2 | 2.2 | 2.7 | 1.9 |
| Pb | 1.3 | 1.0 | 8.7 | 0.8 | 0.9 | 1.9 | 20.0 | 19.3 | 17.6 | 19.3 | 22.3 | 21.9 | 23.0 | 19.2 |
| Th | 0.6 | 0.6 | 0.6 | 1.2 | 0.9 | 1.2 | 11.2 | 6.3 | 9.2 | 8.3 | 25.9 | 32.8 | 36.3 | 24.8 |
| U | 0.1 | 0.2 | 0.1 | 0.3 | 0.3 | 0.3 | 2.1 | 0.7 | 2.2 | 1.3 | 3.1 | 3.7 | 3.3 | 3.7 |
| Mg# | 65.0 | 62.8 | 62.8 | 45.5 | 52.0 | 54.9 | 49.2 | 47.2 | 43.5 | 47.6 | 46.2 | 45.9 | 46.9 | 46.9 |
| Eu/Eu* | 0.34 | 0.32 | 0.34 | 0.30 | 0.31 | 0.29 | 0.27 | 0.35 | 0.26 | 0.36 | 0.16 | 0.14 | 0.14 | 0.17 |
| $La_N/Yb_N$ | 1.7 | 1.7 | 1.6 | 1.7 | 1.6 | 1.5 | 16.0 | 16.0 | 7.6 | 26.7 | 11.2 | 12.7 | 8.7 | 14.8 |
| Nb/Ta | 15.4 | 15.6 | 15.5 | 15.9 | 15.9 | 15.8 | 11.6 | 14.4 | 15.3 | 11.2 | 9.0 | 9.2 | 7.4 | 11.9 |
| Sr/Y | 6.4 | 7.9 | 7.4 | 4.0 | 6.3 | 0.9 | 25.2 | 37.5 | 19.5 | 54.0 | 4.2 | 4.0 | 3.4 | 5.9 |
| Rb/Sr | 0.1 | 0.0 | 0.1 | 0.0 | 0.0 | 0.6 | 0.3 | 0.2 | 0.1 | 0.3 | 1.1 | 1.0 | 1.2 | 0.7 |
| $CaO/Na_2O$ | 2.1 | 2.7 | 2.8 | 2.8 | 2.6 | 9.0 | 1.0 | 0.9 | 1.4 | 0.9 | 0.9 | 0.8 | 0.8 | 1.2 |
| $T_{Zr}$ | | | | | | | 782.5 | 778.9 | 764.1 | 768.2 | 795.7 | 815.8 | 824.2 | 831.2 |

Major-oxide concentrations in wt.%, original XRF totals given.
$TFe_2O_3$ = total Fe as $Fe_2O_3$.
Mg# = 100 Mg/(Mg + Fe).
Trace-element concentrations in ppm by weight.
$T_{Zr}$, zircon saturation thermometer (Watson and Harrison, 1983).

with partial melting, and yielded a concordant U–Pb age 417 ± 2 Ma (zircon rims, Wang et al., 2013).

## 3. Previous studies of early Paleozoic magmatism

Extensive Silurian–Devonian granitoid intrusive and minor mafic rocks are distributed in the Qimantagh region. The mafic–ultramafic rocks exhibit characteristics of formation within an extensional setting. These mafic/ultramafic rocks have U–Pb zircon ages of 405 ± 1 Ma (Wang et al., 2010) and 403 ± 7 Ma (Chen et al., 2006). Qi et al. (2013) and Bao et al. (2013) also documented a suite of 380 ± 2 Ma (U–Pb zircon) basic dyke swarms in the Qimantagh. New geochemical and geochronological studies suggest that the granitoid rocks show the characteristics of I-type granites at 485–462 Ma (Cui, 2011; Li et al.,

| Yusupuleke pluton | | | | | | Bagetuokayi pluton | | | | |
|---|---|---|---|---|---|---|---|---|---|---|
| Aplitic dyke | | | Enclave | | | Monzogranite | | | | |
| 06A-67-1 | 06A-67-2 | 06A-67-3 | 06A-69 | 06A-70 | 06A-66 | 10A-07/1 | 10A-07/2 | 10A-07/3 | 10A-07/4 | 10A-07/5 |
| 70.2 | 70.3 | 70.7 | 50.5 | 57.3 | 53.4 | 75.6 | 74.6 | 74.8 | 76.0 | 75.4 |
| 0.24 | 0.26 | 0.26 | 1.18 | 0.81 | 1.26 | 0.04 | 0.04 | 0.04 | 0.04 | 0.03 |
| 15.4 | 15.7 | 15.2 | 16.7 | 14.8 | 17.4 | 14.1 | 14.4 | 14.5 | 14.1 | 14.3 |
| 2.59 | 2.53 | 2.61 | 12.38 | 9.15 | 9.37 | 0.75 | 0.82 | 0.83 | 0.78 | 0.77 |
| 0.04 | 0.04 | 0.04 | 0.21 | 0.17 | 0.15 | 0.05 | 0.04 | 0.04 | 0.04 | 0.03 |
| 0.91 | 0.90 | 0.89 | 4.03 | 3.23 | 3.97 | 0.09 | 0.08 | 0.09 | 0.09 | 0.08 |
| 3.01 | 3.02 | 2.96 | 5.30 | 3.04 | 5.43 | 0.54 | 0.46 | 0.60 | 0.48 | 0.43 |
| 3.61 | 3.84 | 3.89 | 4.17 | 2.00 | 3.61 | 3.87 | 3.89 | 3.77 | 3.85 | 3.86 |
| 2.58 | 2.65 | 2.64 | 2.57 | 7.79 | 3.89 | 4.25 | 4.35 | 4.39 | 3.96 | 4.37 |
| 0.11 | 0.11 | 0.11 | 0.35 | 0.20 | 0.30 | 0.13 | 0.12 | 0.13 | 0.13 | 0.13 |
| 0.90 | 0.82 | 0.67 | 2.85 | 1.01 | 1.47 | 0.83 | 0.77 | 1.06 | 0.98 | 0.86 |
| 99.5 | 99.5 | 98.9 | 100.3 | 99.5 | 100.2 | 100.3 | 99.5 | 100.3 | 100.4 | 100.3 |
| - | - | - | - | - | - | 152 | 124 | 184 | 145 | 164 |
| 1.5 | 2.7 | 2.9 | 2.5 | 6.3 | 6.1 | 11.0 | 9.5 | 12.6 | 7.6 | 7.5 |
| 3.7 | 5.5 | 5.5 | 5.2 | 22.2 | 21.1 | 2.7 | 2.6 | 2.7 | 2.8 | 2.6 |
| 14.2 | 27.9 | 28.0 | 31.3 | 91.7 | 138.4 | 1.2 | 0.8 | 0.6 | 0.6 | 0.4 |
| 7.0 | 6.0 | 5.7 | 8.0 | 60.5 | 28.2 | 1.4 | 0.6 | 0.7 | 5.9 | 0.6 |
| 126.8 | 3.3 | 3.6 | 139.1 | 60.5 | 42.9 | 176.4 | 153.5 | 153.2 | 179.9 | 187.1 |
| 3.8 | 1.6 | 1.6 | 4.7 | 53.5 | 26.3 | 2.3 | 0.5 | 0.6 | 4.7 | 0.4 |
| 4.1 | 35.9 | 37.6 | 2.4 | 20.2 | 13.4 | 0.7 | 0.7 | 0.8 | 1.4 | 0.9 |
| 36.5 | 18.4 | 18.6 | 38.6 | 11.6 | 110.5 | 20.3 | 20.8 | 18.7 | 18.1 | 17.6 |
| 20.3 | 1.5 | 1.5 | 18.5 | 125.4 | 25.8 | 20.0 | 19.5 | 20.6 | 20.1 | 19.8 |
| - | - | - | - | 24.5 | - | 2.1 | 1.9 | 1.9 | 2.0 | 2.0 |
| 311.2 | 157.7 | 173.5 | 157.6 | 427.9 | 253.0 | 318.7 | 289.6 | 330.8 | 298.9 | 315.6 |
| 71.4 | 315.2 | 305.3 | 314.0 | 82.1 | 181.4 | 5.9 | 6.2 | 7.6 | 6.6 | 5.6 |
| 42.4 | 17.5 | 18.9 | 17.3 | 88.6 | 35.3 | 14.8 | 13.8 | 13.9 | 13.0 | 11.5 |
| 115.6 | 155.1 | 143.6 | 148.9 | 280.9 | 304.1 | 27.8 | 28.0 | 30.5 | 28.5 | 28.1 |
| 7.3 | 15.1 | 15.5 | 15.1 | 35.7 | 26.0 | 6.5 | 7.0 | 8.3 | 9.2 | 9.3 |
| 4.9 | 12.0 | 14.2 | 11.8 | 20.1 | 13.9 | 37.3 | 27.4 | 37.9 | 33.7 | 35.2 |
| 601.3 | 451.8 | 426.7 | 448.1 | 506.3 | 335.2 | 8.7 | 7.2 | 10.3 | 9.2 | 5.7 |
| 34.9 | 31.4 | 23.5 | 31.2 | 14.9 | 28.6 | 4.0 | 3.0 | 3.4 | 3.5 | 3.1 |
| 73.6 | 58.2 | 42.3 | 57.5 | 49.8 | 58.9 | 10.2 | 7.2 | 8.1 | 8.8 | 6.9 |
| 8.0 | 5.9 | 4.3 | 5.9 | 8.3 | 6.9 | 1.2 | 0.8 | 0.9 | 1.0 | 0.8 |
| 30.8 | 21.2 | 15.7 | 21.0 | 42.6 | 27.5 | 4.4 | 2.9 | 3.3 | 3.5 | 2.9 |
| 6.8 | 3.8 | 3.0 | 3.7 | 12.9 | 5.9 | 1.5 | 1.1 | 1.1 | 1.3 | 1.0 |
| 1.0 | 0.8 | 0.7 | 0.7 | 0.9 | 0.9 | 0.0 | 0.0 | 0.0 | 0.0 | 0.0 |
| 6.7 | 3.4 | 2.8 | 3.5 | 13.1 | 5.9 | 1.6 | 1.2 | 1.3 | 1.3 | 1.1 |
| 1.1 | 0.5 | 0.5 | 0.5 | 2.3 | 0.9 | 0.4 | 0.3 | 0.3 | 0.3 | 0.3 |
| 7.1 | 2.9 | 2.8 | 2.9 | 14.6 | 5.6 | 2.4 | 2.1 | 2.1 | 2.0 | 1.8 |
| 1.5 | 0.6 | 0.6 | 0.6 | 3.0 | 1.1 | 0.4 | 0.4 | 0.4 | 0.4 | 0.3 |
| 4.3 | 1.6 | 1.7 | 1.6 | 8.7 | 3.4 | 1.4 | 1.3 | 1.3 | 1.2 | 1.1 |
| 0.7 | 0.3 | 0.3 | 0.2 | 1.4 | 0.6 | 0.3 | 0.2 | 0.2 | 0.2 | 0.2 |
| 4.0 | 1.7 | 1.9 | 1.6 | 8.7 | 3.6 | 1.9 | 1.7 | 1.8 | 1.7 | 1.5 |
| 0.6 | 0.2 | 0.3 | 0.2 | 1.4 | 0.6 | 0.3 | 0.2 | 0.3 | 0.2 | 0.2 |
| 3.3 | 3.9 | 3.7 | 3.8 | 7.6 | 7.1 | 1.3 | 1.2 | 1.4 | 1.3 | 1.3 |
| 1.0 | 1.5 | 1.7 | 1.9 | 2.0 | 1.4 | 2.3 | 1.7 | 2.4 | 2.4 | 2.2 |
| 37.9 | 16.9 | 16.1 | 15.9 | 35.3 | 24.3 | 18.8 | 17.9 | 17.0 | 15.8 | 14.8 |
| 23.7 | 14.2 | 13.5 | 12.5 | 7.6 | 10.0 | 5.1 | 3.6 | 4.3 | 4.5 | 4.0 |
| 2.3 | 3.0 | 3.2 | 2.7 | 2.1 | 3.4 | 4.1 | 4.9 | 5.4 | 4.1 | 4.3 |
| 45.0 | 45.3 | 44.3 | 43.1 | 45.1 | 49.7 | 21.9 | 18.5 | 20.2 | 21.2 | 19.5 |
| 0.15 | 0.22 | 0.25 | 0.21 | 0.07 | 0.15 | 0.02 | 0.02 | 0.02 | 0.02 | 0.02 |
| 6.3 | 13.6 | 8.9 | 14.1 | 1.2 | 5.7 | 1.5 | 1.2 | 1.4 | 1.5 | 1.5 |
| 7.7 | 10.0 | 9.0 | 8.1 | 17.9 | 18.6 | 2.8 | 4.2 | 3.5 | 3.8 | 4.2 |
| 1.7 | 18.1 | 16.1 | 18.1 | 0.9 | 5.1 | 0.4 | 0.4 | 0.5 | 0.5 | 0.5 |
| 4.4 | 0.5 | 0.6 | 0.5 | 5.2 | 1.4 | 54.3 | 46.9 | 43.4 | 45.2 | 56.6 |
| 0.8 | 0.8 | 0.8 | 1.3 | 1.5 | 1.5 | 0.1 | 0.1 | 0.2 | 0.1 | 0.1 |
| 759.3 | 782.3 | 773.2 | 713.7 | 781.8 | 776.9 | 664.9 | 665.8 | 671.9 | 669.6 | 666.6 |

2013) and A-type granites at 441–380 Ma (e.g., Chen et al., 2006; Gao and Li, 2011; Guo et al., 2011; Li et al., 2013; Wang et al., 2012; Wu et al., 2007). Many researchers suggested that granitoids with ages of 485–462 Ma were formed in an island arc setting (Cui, 2011; Li et al., 2013). Some intrusions are exposed along the Baiganhu shear faults trending NE that formed at ca. 413–412 Ma (Ar–Ar age dating; Feng et al., 2013) and recent mapping in the Qimantagh identified a belt of 445–440 Ma basaltic and rhyolitic rocks (Wang et al., 2012).

Voluminous granitic and mafic magmas were intruded in the southern segment of the Altyn Tagh along the major shear zones during early Paleozoic orogenesis (Fig. 1c). Mafic–ultramafic rocks are widely distributed along the southern margin of the South Altyn. The mafic–ultramafic rocks consist of serpentinized dunite, harzburgite, mafic volcanic

rock, and gabbro. Some mafic volcanic rocks show geochemical characteristics similar to E-MORBs (Wang et al., 1999) and N-MORBs (Li et al., 2009), with whole-rock Sm–Nd isochron ages of 493–481 Ma (Liu et al., 1998) and a U–Pb zircon age of 501 ± 2 Ma obtained on gabbro (Li et al., 2009). These rocks were interpreted as a mélange of ophiolitic rocks (Li et al., 2009; Liu et al., 1998); however, new geochemical and geochronological studies suggest that at least some of them are parts of layered igneous intrusions formed in an extensional setting. The mafic and ultramafic rocks have U–Pb zircon ages of 467 ± 1 Ma (Ma et al., 2011) and 445 ± 1 Ma (Dong et al., 2011). In the Qingshuiquan area, the mafic–ultramafic rocks intrude marbles that are also observed as xenoliths in the intruding units (Ma et al., 2011). South Altyn consists of numerous granitoid batholiths and plutons of varying size (Fig. 1c). Based on the most precise U–Pb zircon ages (Fig. 1c), the South Altyn early Paleozoic granitic rocks were emplaced over a time span of 500 to 385 Ma (Liu et al., 2013). They can be broadly sub-divided into three distinct granitic suites (Fig. 1c): (1) granite with U–Pb zircon age of 497 ± 2 Ma, that was derived from melting of thickened lower continental crust (Sun et al., 2012); (2) High-potassium calc-alkaline granitic plutons, related to transpressional tectonics, dated between 480 and 440 Ma (Cao et al., 2010; Cowgill et al., 2003; Yang et al., 2012); and (3) A-type granitic series suite emplaced between 426 and 385 Ma (Liu et al., 2013). Yang et al. (2012) and Liu et al. (2013) suggest that these early Paleozoic granites of the South Altyn are related to exhumation of deeply subducted HP/UHP metamorphic rocks. Cui (2011) noted that the entire South Altyn was affected by E–W trending and S-dipping high-angle faults that formed at ~468–412 Ma (Ar–Ar age dating) and suggested that the faulting was related to early Paleozoic orogenesis. Volumes of calc-alkaline granitic rocks and HP/UHP metamorphic rocks appear to be genetically related to the main sites of deformation within the shear regime (Fig. 1c).

Geochronological data of the Qimantagh and South Altyn indicate that the mafic rocks are also contemporaneous with a suite of felsic igneous rocks. These bimodal suites are thought to have developed during lithospheric extension following continent–continent collision; however, the geodynamic significance of these post-collisional granitic associations and mafic melts has not been fully established. In the present study, the Mangya mafic rocks, Yusupuleke (YP) and Bagetuokayi plutons (BP) are investigated in order to better understand the timing and nature of post-collisional magmatism.

## 4. Sample location and petrography

In the study area (Fig. 2), there are serpentinized peridotites, diabases, metabasalts and tuff represented in the mafic–ultramafic belt along the Altyn Tagh fault. These mafic–ultramafic rocks are associated with coeval granitic rocks. The Yusupuleke pluton outcrops at the north side of the mafic–ultramafic belt and is aligned in an E–W direction. The Bagetuokayi pluton outcrops in the southern region (Fig. 2).

The basalts occur as pillow lavas and massive flows. The basalts are interlayered with tuffs and cross-cut by veinlets filled with chlorite and calcite. The studied basalt (sample 10A-06/1) is represented by amygdaloidal ophitic basalt, mostly transformed into metabasalt (Fig. 3a). Mineral assemblages are characterized by feldspar and pyroxene (augite). The basalts are, to varying degrees, altered to chlorite and/or epidote. The studied diabase samples (10A-06/7, 10A-06/8 and 10A-06/9, 10A-06/10 and 10A-06/11) show mainly ophitic to subophitic textures with medium-grained size. Mineral assemblages in the diabase include plagioclase, clinopyroxene, amphibole, and accessory ilmenite, zircon and apatite. The diabase samples are slightly to moderately affected by hydrothermal metamorphism, as exhibited by albitization and prehnitization of plagioclase.

The Yusupuleke pluton (YP) is a porphyritic granodiorite and monzogranite with an association of microgranular enclaves. Some aplitic dykes intruded in the coarse grained monzogranites. Pink gray-colored granite contains fine-grained enclaves displaying igneous textures (Wang et al., 2008). The granodiorite consists of plagioclase (55–60%), quartz (20–25%), K-feldspar (15–18%), amphibole (1–5%) and biotite (1–2%) and subordinate amounts of apatite, zircon, titanite and magnetite with a medium-grained granitic texture. The monzogranites are coarse grained, porphyritic-like, poikilitic texture with mineral assemblages that include microcline with rapikivi textures (35–45%, phenocrysts up to 10 mm in length; Fig. 3b), plagioclase (25–30%), quartz (20–22%), biotite (2–5%) and hornblende (1–5%). Accessory minerals include apatite, zircon and titanite crystals up to 2 mm in length. Hornblende, quartz and plagioclase occurred as xenocrysts in the cores of megacrystic alkali feldspar. These textures are commonly associated with magma mixing (Wang et al., 2008). The enclaves are darker and richer in mafic minerals than the host granite. The enclaves show rounded, elongate or irregular shapes in the host granite with sharp contact with the host granite. They range in size from a few centimeters to decimeters. Some elongated enclaves define a distinct magmatic foliation (Fig. 3c). Enclaves are quartz monzonites and quartz syenites. They have fine-grained, poikilitic-equigranular textures. Enclaves consist of variable proportions of plagioclase (30–50%), quartz (5–10%), hornblende (15–25%), perthite (10–15%), biotite (10–25%) and accessory minerals of titanite, apatite and zircons. Some biotite crystals are altered to chlorite in enclaves. Prismatic apatite is also present and suggests that cooling was rapid (Wang et al., 2008). Some enclaves have a few larger feldspar phenocrysts, indicating mingling of dioritic and granite magmas (e.g. Hibbard, 1991). The size of quartz and feldspar crystals is up to 2 mm in length. Narrow aplitic dykes intrude the monzogranites. The dykes emplaced into semi-consolidated granitic material of the porphyritic YP monzogranite suggest that they are feeder dykes to that pluton. Aplitic dykes are fine-grained, porphyritic-like texture tonalites. They consist of plagioclase, biotite and quartz. Accessory minerals include titanite, apatite, zircon and opaque phases. Zoned plagioclase is albite-rich with $An_{30–50}$. Some feldspar phenocrysts show rapakivi texture and are up to 10 mm (Fig. 3d). Textural and mineralogical assemblages found in the YP such as rapakivi textures, zoned plagioclase, acicular apatite and K-feldspar megacrysts indicate a magma mixing processes (Wang et al., 2008).

The Bagetuokayi pluton crops out in a 1000 m long and 200 m wide lens in the south, and is composed of monzogranite. The rock consists of plagioclase (50–55%), K-feldspar (17–20%), quartz (24–28%), muscovite (3–5%) and biotite (1–2%), with a medium-grained granitic texture. Muscovites are commonly anhedral and interstitial to both feldspar and quartz.

## 5. Analytical methods

### 5.1. Major and trace elemental analyses

Samples were analyzed at the State Key Laboratory of Continental Dynamics of Northwest University in Xi'an, China. Fresh chips of whole rock samples were powdered to a 200 mesh-size using a tungsten carbide ball mill. Major and trace elements were analyzed by XRF (Rikagu RIX 2100) and ICP-MS (Agilent 7500a), respectively. Analyses of USGS and Chinese national rock standards (BCR-2, GSR-1 and GSR-3) indicate that analytical precision and accuracy for major elements are generally better than 5%. For trace element analysis, sample powders were digested using an HF + $HNO_3$ mixture in high-pressure Teflon bombs at 190 °C for 48 h. Analytical precision is better than 10% for most trace elements. The geochemical data are shown in Table 1.

### 5.2. Zircon U–Pb isotope analysis

Zircon grains were separated from the representative samples by heavy-liquid and magnetic techniques followed by hand picking under a binocular microscope. Zircon grains were handpicked and mounted in epoxy resin disks, and then polished and coated with


**Fig. 4.** Representative CL images of zircons from dated mafic and granitic rocks. Ic: inherited core; c: core; r: rim. See the details in the text.

carbon. Cathodoluminescence (CL) images of the zircons were taken using a Mono CL3 + microprobe prior to U–Pb dating at the State Key Laboratory of Continental Dynamics at Northwest University, China. U–Pb data were obtained using an Agilent 7500a ICP-MS. The ICP-MS equipped with unique Shield Torch brought about higher sensitivity. The used GeoLas 200 M laser ablation system consists of ComPex102 (193 nm ArF-excimer laser, Lambda Physik) and optical system (MicroLas). During analysis, the spot diameter was 33 μm. ICP-MS operating conditions were generally optimized using continuous ablation of reference glass NIST SRM 610, to provide maximum sensitivity for the high masses while maintaining low oxide formation and low background. U, Th and Pb concentrations were calibrated by using $^{29}Si$ as the internal standard and NIST SRM 610 as the external standard. $^{207}Pb/^{206}Pb$ and $^{206}Pb/^{238}U$ ratios were calculated using the GLITTER 4.0 program, and then corrected using the Harvard zircon 91500 as the external standard. U–Pb ages were calculated by the ISOPLOT program (Ludwig, 2003). The detailed instrumental parameters and analytical procedures can be referred to Yuan et al. (2008).

## 6. Results

### 6.1. LA-ICP-MS U–Pb zircon geochronology

We analyzed six samples in this study. These samples contain complex magmatic zircons (Fig. 4). The results are listed in Table 2 and plotted in Fig. 5.

Sample 11SA-3 was collected from the diabases. CL images show that all zircon crystals have banded structure (Fig. 4), as is common in zircon from mafic igneous rocks (Hoskin, 2000). Three zircons give older $^{206}Pb/^{238}U$ ages between 460 ± 2 and 463 ± 3 Ma and one zircon yields the youngest age (439 ± 4 Ma). A main group of nearly concordant analyses (5 analyses) gives $^{206}Pb/^{238}U$ ages between 449 ± 3 and 455 ± 3 Ma and yields a weighted mean $^{206}Pb/^{238}U$ age of 453 ± 5 Ma (Fig. 5a; MSWD = 1.7). The weighted mean age is regarded as the best estimate for the crystallization age of the diabases.

Sample 10A-6-12 was collected from the YP granodiorite and contained zircons with well-developed concentric oscillatory zoned or molten core and thin light luminescent rim (Fig. 4). The rims were quite thin and all analyses were carried out on the core regions of the zircons. The $^{206}Pb/^{238}U$ ages were dispersed much more than expected from the analytical uncertainties, indicative in some cases of major radiogenic Pb loss. Eleven concordant core analyses yield a weighted mean $^{206}Pb/^{238}U$ age of 446 ± 3 Ma (Fig. 5b; MSWD = 2.2), that is interpreted as the best estimate for the crystallization age of the sample.

Sample 06A-68 is from the monzogranite phase of the YP. Zircons generally consist of bright or gray cores surrounded by dark rims (Fig. 4). Some cores are subhedral, simple banding and deeply embayed, apparently by partial dissolution (Fig. 4). Rims show fine, concentric oscillatory zoning (Fig. 4). Three concordant core analyses yield a weighted mean $^{206}Pb/^{238}U$ age of 431 ± 9 Ma (Fig. 5c; MSWD = 1.7) Four concordant rim analyses yield a statistically identical weighted mean $^{206}Pb/^{238}U$ age of 432 ± 4 Ma (Fig. 5d; MSWD = 0.11). The similar age populations suggest that both domains formed at the same time. There is no systematic relationship in the core and rim sample between the age populations and Th/U ratios. Both domains contain euhedral zoning that is consistent with zircon growth in a magmatic fluid, while the dark rims could be attributed to the change of element concentration. Therefore, it is our estimate that these represent the crystallization age of the YP monzogranite.

**Table 2**
LA-ICPMS U–Th–Pb isotope data of zircon.

| Analysis | Pb (ppm) | Th (ppm) | U (ppm) | Th/U | $^{207}Pb/^{206}Pb$ | 1 σ | $^{207}Pb/^{235}U$ | 1σ | $^{206}Pb/^{238}U$ | 1σ | $^{207}Pb/^{206}Pb$ | 1σ (Ma) | $^{207}Pb/^{235}U$ | 1σ (Ma) | $^{206}Pb/^{238}U$ | 1 σ (Ma) | Concordance[a] | Type[b] |
|---|---|---|---|---|---|---|---|---|---|---|---|---|---|---|---|---|---|---|
| *Sample 11SA-3* | | | | | | | | | | | | | | | | | | |
| 11SA-3-1 | 67 | 489 | 719 | 0.68 | 0.060410 | 0.000710 | 0.615890 | 0.004920 | 0.073940 | 0.000410 | 618 | 9 | 487 | 3 | 460 | 2 | 94 | |
| 11SA-3-2 | 81 | 556 | 845 | 0.66 | 0.057210 | 0.000960 | 0.575040 | 0.009070 | 0.072900 | 0.000430 | 500 | 38 | 461 | 6 | 454 | 3 | 98 | |
| 11SA-3-3 | 19 | 145 | 201 | 0.72 | 0.059890 | 0.001400 | 0.595060 | 0.012740 | 0.072070 | 0.000540 | 600 | 33 | 474 | 8 | 449 | 3 | 95 | |
| 11SA-3-4 | 78 | 918 | 733 | 1.25 | 0.059350 | 0.000740 | 0.601870 | 0.005370 | 0.073550 | 0.000420 | 580 | 10 | 478 | 3 | 458 | 3 | 96 | |
| 11SA-3-5 | 30 | 198 | 292 | 0.68 | 0.056090 | 0.002570 | 0.544860 | 0.024440 | 0.070460 | 0.000670 | 456 | 104 | 442 | 16 | 439 | 4 | 99 | |
| 11SA-3-6 | 55 | 415 | 606 | 0.69 | 0.058360 | 0.000770 | 0.596300 | 0.005900 | 0.074110 | 0.000430 | 543 | 12 | 475 | 4 | 461 | 3 | 97 | |
| 11SA-3-7 | 57 | 318 | 636 | 0.50 | 0.058390 | 0.000750 | 0.598870 | 0.005630 | 0.074400 | 0.000430 | 544 | 11 | 477 | 4 | 463 | 3 | 97 | |
| 11SA-3-8 | 37 | 450 | 356 | 1.27 | 0.056720 | 0.000880 | 0.572330 | 0.007290 | 0.073200 | 0.000450 | 481 | 17 | 460 | 5 | 455 | 3 | 99 | |
| 11SA-3-9 | 11 | 87 | 124 | 0.70 | 0.057320 | 0.001850 | 0.570390 | 0.017910 | 0.072170 | 0.000550 | 504 | 73 | 458 | 12 | 449 | 3 | 98 | |
| *Sample 10a-6-12* | | | | | | | | | | | | | | | | | | |
| 10A-6-12-1 | 64 | 372 | 742 | 0.50 | 0.058490 | 0.000780 | 0.570160 | 0.005830 | 0.070700 | 0.000410 | 548 | 13 | 458 | 4 | 440 | 2 | 104 | |
| 10A-6-12-2 | 125 | 801 | 1372 | 0.58 | 0.056920 | 0.000710 | 0.566160 | 0.005260 | 0.072150 | 0.000410 | 488 | 11 | 456 | 3 | 449 | 2 | 102 | |
| 10A-6-12-3 | 102 | 788 | 1097 | 0.72 | 0.057650 | 0.000710 | 0.566750 | 0.005080 | 0.071310 | 0.000400 | 516 | 10 | 456 | 3 | 444 | 2 | 103 | |
| 10A-6-12-4 | 110 | 765 | 1219 | 0.63 | 0.057550 | 0.000680 | 0.564980 | 0.004750 | 0.071220 | 0.000390 | 513 | 9 | 455 | 3 | 444 | 2 | 102 | |
| 10A-6-12-5 | 35 | 180 | 398 | 0.45 | 0.057280 | 0.000920 | 0.569570 | 0.007650 | 0.072120 | 0.000450 | 502 | 19 | 458 | 5 | 449 | 3 | 102 | |
| 10A-6-12-6 | 69 | 377 | 772 | 0.49 | 0.057170 | 0.000750 | 0.568190 | 0.005680 | 0.072100 | 0.000410 | 498 | 12 | 457 | 4 | 449 | 2 | 102 | |
| 10A-6-12-7 | 78 | 398 | 838 | 0.48 | 0.061720 | 0.001090 | 0.609340 | 0.010110 | 0.071600 | 0.000430 | 664 | 39 | 483 | 6 | 446 | 3 | 108 | |
| 10A-6-12-8 | 149 | 809 | 1596 | 0.51 | 0.062030 | 0.001000 | 0.610000 | 0.009210 | 0.071330 | 0.000410 | 675 | 35 | 484 | 6 | 444 | 2 | 109 | |
| 10A-6-12-9 | 52 | 184 | 524 | 0.35 | 0.056330 | 0.001040 | 0.560790 | 0.009070 | 0.072220 | 0.000480 | 465 | 24 | 452 | 6 | 450 | 3 | 100 | |
| 10A-6-12-10 | 102 | 754 | 1069 | 0.70 | 0.058890 | 0.001080 | 0.579360 | 0.009980 | 0.071360 | 0.000430 | 563 | 41 | 464 | 6 | 444 | 3 | 105 | |
| 10A-6-12-11 | 123 | 1383 | 1226 | 1.13 | 0.061150 | 0.000720 | 0.599380 | 0.004880 | 0.071100 | 0.000390 | 645 | 9 | 477 | 3 | 443 | 2 | 108 | |
| 10A-6-12-12 | 99 | 524 | 1138 | 0.46 | 0.060260 | 0.000840 | 0.583970 | 0.007470 | 0.070290 | 0.000400 | 613 | 31 | 467 | 5 | 438 | 2 | 107 | |
| 10A-6-12-13 | 55 | 405 | 578 | 0.70 | 0.059490 | 0.001280 | 0.584200 | 0.012010 | 0.071220 | 0.000460 | 585 | 48 | 467 | 8 | 443 | 3 | 105 | |
| 10A-6-12-14 | 92 | 771 | 780 | 0.99 | 0.060620 | 0.001950 | 0.596920 | 0.018780 | 0.071410 | 0.000470 | 626 | 71 | 475 | 12 | 445 | 3 | 107 | |
| 10A-6-12-15 | 95 | 579 | 800 | 0.72 | 0.059230 | 0.002210 | 0.594250 | 0.021790 | 0.072770 | 0.000490 | 576 | 83 | 474 | 14 | 453 | 3 | 105 | |
| 10A-6-12-16 | 125 | 1244 | 1314 | 0.95 | 0.062540 | 0.000720 | 0.602620 | 0.004760 | 0.069890 | 0.000390 | 693 | 8 | 479 | 3 | 435 | 2 | 110 | |
| 10A-6-12-17 | 51 | 220 | 556 | 0.39 | 0.056710 | 0.001090 | 0.552210 | 0.010050 | 0.070630 | 0.000430 | 480 | 43 | 446 | 7 | 440 | 3 | 101 | |
| 10A-6-12-18 | 151 | 1030 | 1661 | 0.62 | 0.068650 | 0.000970 | 0.665390 | 0.008560 | 0.070300 | 0.000410 | 888 | 30 | 518 | 5 | 438 | 2 | 118 | |
| 10A-6-12-19 | 71 | 373 | 611 | 0.61 | 0.106650 | 0.001250 | 1.174370 | 0.009520 | 0.079860 | 0.000460 | 1743 | 7 | 789 | 4 | 495 | 3 | 159 | |
| 10A-6-12-20 | 92 | 1168 | 842 | 1.39 | 0.061190 | 0.001640 | 0.593810 | 0.015360 | 0.070380 | 0.000480 | 646 | 59 | 473 | 10 | 438 | 3 | 108 | |
| 10A-6-12-21 | 205 | 2245 | 1931 | 1.16 | 0.065900 | 0.000800 | 0.642000 | 0.005590 | 0.070650 | 0.000400 | 803 | 9 | 504 | 3 | 440 | 2 | 115 | |
| 10A-6-12-22 | 92 | 558 | 686 | 0.81 | 0.157390 | 0.001810 | 1.725190 | 0.013210 | 0.079500 | 0.000460 | 2428 | 6 | 1018 | 5 | 493 | 3 | 206 | |
| 10A-6-12-23 | 58 | 345 | 617 | 0.56 | 0.057340 | 0.001290 | 0.571550 | 0.012300 | 0.072300 | 0.000480 | 505 | 51 | 459 | 8 | 450 | 3 | 102 | |
| 10A-6-12-24 | 96 | 557 | 1010 | 0.55 | 0.076250 | 0.000930 | 0.754820 | 0.006540 | 0.071790 | 0.000410 | 1102 | 9 | 571 | 4 | 447 | 2 | 128 | |
| 10A-6-12-25 | 31 | 210 | 331 | 0.63 | 0.055610 | 0.001600 | 0.543720 | 0.015140 | 0.070910 | 0.000520 | 437 | 66 | 441 | 10 | 442 | 3 | 100 | |
| 10A-6-12-26 | 181 | 2355 | 1731 | 1.36 | 0.068700 | 0.000770 | 0.673220 | 0.005010 | 0.071070 | 0.000390 | 890 | 7 | 523 | 3 | 443 | 2 | 118 | |
| 10A-6-12-27 | 111 | 641 | 1214 | 0.53 | 0.055710 | 0.001030 | 0.549110 | 0.009580 | 0.071490 | 0.000430 | 441 | 42 | 444 | 6 | 445 | 3 | 100 | |
| 10A-6-12-28 | 309 | 4566 | 2731 | 1.67 | 0.057200 | 0.001460 | 0.556270 | 0.013700 | 0.070540 | 0.000460 | 499 | 57 | 449 | 9 | 439 | 3 | 102 | |
| *Sample 06a-68* | | | | | | | | | | | | | | | | | | |
| 06A-68-1 | 148 | 530 | 1951 | 0.27 | 0.057490 | 0.001267 | 0.530104 | 0.012088 | 0.066838 | 0.001061 | 509 | 53 | 432 | 8 | 417 | 6 | 96 | c |
| 06A-68-2 | 89 | 1087 | 903 | 1.20 | 0.062446 | 0.001047 | 0.585985 | 0.011266 | 0.068405 | 0.001266 | 700 | 35 | 468 | 7 | 427 | 8 | 90 | r |
| 06A-68-3 | 92 | 438 | 1136 | 0.39 | 0.057481 | 0.000908 | 0.550396 | 0.009878 | 0.069493 | 0.000857 | 509 | 33 | 445 | 6 | 433 | 5 | 97 | r |
| 06A-68-4 | 110 | 636 | 1363 | 0.47 | 0.066782 | 0.000912 | 0.617553 | 0.009015 | 0.066838 | 0.000401 | 831 | | 488 | 6 | 417 | 2 | 84 | r |
| 06A-68-5 | 39 | 141 | 489 | 0.29 | 0.061551 | 0.001320 | 0.585707 | 0.012391 | 0.068890 | 0.000452 | 657 | 46 | 468 | 8 | 429 | 3 | 91 | r |
| 06A-68-6 | 57 | 472 | 621 | 0.76 | 0.056895 | 0.001539 | 0.548368 | 0.015373 | 0.069661 | 0.000539 | 487 | 59 | 444 | 10 | 434 | 3 | 97 | c |
| 06A-68-7 | 95 | 516 | 1177 | 0.44 | 0.062282 | 0.001006 | 0.572684 | 0.010534 | 0.066453 | 0.000478 | 683 | 33 | 460 | 7 | 415 | 3 | 89 | r |
| 06A-68-8 | 76 | 287 | 956 | 0.30 | 0.055523 | 0.000738 | 0.530948 | 0.007497 | 0.069242 | 0.000386 | 432 | | 432 | 5 | 432 | 2 | 99 | c |
| 06A-68-9 | 95 | 676 | 1100 | 0.61 | 0.063137 | 0.000980 | 0.594552 | 0.012976 | 0.068168 | 0.001074 | 722 | 33 | 474 | 8 | 425 | 6 | 89 | c |
| 06A-68-10 | 48 | 313 | 548 | 0.57 | 0.055290 | 0.001383 | 0.522109 | 0.013467 | 0.068455 | 0.000426 | 433 | 56 | 427 | 9 | 427 | 3 | 99 | c |
| 06A-68-11 | 168 | 832 | 2030 | 0.41 | 0.076989 | 0.000634 | 0.704017 | 0.008099 | 0.066247 | 0.000541 | 1120 | 17 | 541 | 5 | 414 | 3 | 73 | r |

| | | | | | | | | | | | | | | | | | | |
|---|---|---|---|---|---|---|---|---|---|---|---|---|---|---|---|---|---|---|
| 06A-68-12 | 66 | 476 | 759 | 0.63 | 0.070874 | 0.002160 | 0.647718 | 0.022374 | 0.065981 | 0.000696 | 954 | 58 | 507 | 14 | 412 | 4 | 79 | c |
| 06A-68-13 | 100 | 540 | 1264 | 0.43 | 0.057436 | 0.000619 | 0.554296 | 0.008937 | 0.069542 | 0.000688 | 509 | 24 | 448 | 6 | 433 | 4 | 96 | r |
| 06A-68-14 | 97 | 476 | 1288 | 0.37 | 0.056384 | 0.000739 | 0.540773 | 0.008172 | 0.069144 | 0.000498 | 478 | 28 | 439 | 5 | 431 | 3 | 98 | r |
| 06A-68-15 | 78 | 934 | 880 | 1.06 | 0.057675 | 0.000922 | 0.552762 | 0.014221 | 0.069015 | 0.001170 | 517 | 35 | 447 | 9 | 430 | 7 | 96 | r |
| *Sample 06a-67* | | | | | | | | | | | | | | | | | | |
| 06A-67-1 | 337 | 653 | 4833 | 0.14 | 0.055479 | 0.000377 | 0.521047 | 0.004778 | 0.067763 | 0.000435 | 432 | 19 | 426 | 3 | 423 | 3 | 99 | r |
| 06A-67-2 | 141 | 578 | 1944 | 0.30 | 0.055716 | 0.000893 | 0.523682 | 0.013512 | 0.067659 | 0.001202 | 443 | 35 | 428 | 9 | 422 | 7 | 98 | r |
| 06A-67-3 | 249 | 569 | 3503 | 0.16 | 0.054694 | 0.000408 | 0.517590 | 0.005525 | 0.068221 | 0.000564 | 398 | 17 | 424 | 4 | 425 | 3 | 99 | r |
| 06A-67-4 | 66 | 376 | 921 | 0.41 | 0.059811 | 0.001114 | 0.521598 | 0.011938 | 0.062815 | 0.000827 | 598 | 34 | 426 | 8 | 393 | 5 | 91 | lc |
| 06A-67-5 | 55 | 313 | 717 | 0.44 | 0.056943 | 0.001017 | 0.525737 | 0.009000 | 0.066653 | 0.000450 | 500 | 39 | 429 | 6 | 416 | 3 | 96 | r |
| 06A-67-6 | 341 | 694 | 4766 | 0.15 | 0.088448 | 0.002857 | 0.783769 | 0.030713 | 0.062776 | 0.000798 | 1392 | 63 | 588 | 17 | 392 | 5 | 60 | r |
| 06A-67-7 | 187 | 807 | 2412 | 0.33 | 0.055329 | 0.000531 | 0.560969 | 0.010613 | 0.072994 | 0.001180 | 433 | −6 | 452 | 7 | 454 | 7 | 99 | lc |
| 06A-67-8 | 198 | 792 | 2652 | 0.30 | 0.054489 | 0.000507 | 0.515555 | 0.009137 | 0.068176 | 0.001026 | 391 | 22 | 422 | 6 | 425 | 6 | 99 | r |
| 06A-67-9 | 475 | 1429 | 7021 | 0.20 | 0.062161 | 0.000400 | 0.533945 | 0.007047 | 0.061821 | 0.000591 | 680 | 15 | 434 | 5 | 387 | 4 | 88 | r |
| 06A-67-10 | 6 | 41 | 72 | 0.57 | 0.056237 | 0.002438 | 0.518329 | 0.021166 | 0.067565 | 0.000834 | 461 | 96 | 424 | 14 | 421 | 5 | 99 | c |
| 06A-67-11 | 76 | 423 | 929 | 0.46 | 0.055753 | 0.000559 | 0.561092 | 0.006155 | 0.072627 | 0.000362 | 443 | 22 | 452 | 4 | 452 | 2 | 99 | lc |
| 06A-67-12 | 383 | 1320 | 5786 | 0.23 | 0.058148 | 0.000511 | 0.501570 | 0.006467 | 0.062214 | 0.000508 | 600 | 19 | 413 | 4 | 389 | 3 | 94 | lc |
| 06A-67-13 | 340 | 562 | 4971 | 0.11 | 0.055928 | 0.000450 | 0.523838 | 0.008319 | 0.067497 | 0.000786 | 450 | 23 | 428 | 6 | 421 | 5 | 98 | r |
| 06A-67-14 | 36 | 238 | 423 | 0.56 | 0.055301 | 0.002381 | 0.560069 | 0.025317 | 0.073051 | 0.000772 | 433 | 96 | 452 | 16 | 455 | 5 | 99 | ic |
| 06A-67-15 | 455 | 764 | 6891 | 0.11 | 0.060054 | 0.000444 | 0.515336 | 0.005148 | 0.061922 | 0.000436 | 606 | 15 | 422 | 3 | 387 | 3 | 91 | r |
| 06A-67-16 | 156 | 550 | 2185 | 0.25 | 0.055745 | 0.000931 | 0.521549 | 0.014392 | 0.067615 | 0.001723 | 443 | 37 | 426 | 10 | 422 | 10 | 98 | c |
| 06A-67-17 | 34 | 219 | 446 | 0.49 | 0.055196 | 0.000904 | 0.516460 | 0.008869 | 0.067582 | 0.000459 | 420 | 37 | 423 | 6 | 422 | 3 | 99 | c |
| 06A-67-18 | 574 | 999 | 9821 | 0.10 | 0.059819 | 0.000379 | 0.516515 | 0.012995 | 0.062029 | 0.001261 | 598 | 13 | 423 | 9 | 388 | 8 | 91 | r |
| 06A-67-19 | 16 | 138 | 183 | 0.75 | 0.082458 | 0.002281 | 0.764627 | 0.018834 | 0.067793 | 0.000811 | 1257 | 21 | 577 | 11 | 423 | 5 | 69 | c |
| 06A-67-20 | 309 | 647 | 4831 | 0.13 | 0.060441 | 0.000365 | 0.519593 | 0.004378 | 0.062060 | 0.000417 | 620 | 13 | 425 | 3 | 388 | 3 | 90 | r |
| 06A-67-21 | 178 | 649 | 2322 | 0.28 | 0.056955 | 0.000884 | 0.568378 | 0.010273 | 0.071989 | 0.000726 | 500 | 35 | 457 | 7 | 448 | 4 | 98 | lc |
| 06A-67-22 | 270 | 739 | 4197 | 0.18 | 0.064064 | 0.000557 | 0.551426 | 0.007665 | 0.062036 | 0.000652 | 743 | 19 | 446 | 5 | 388 | 4 | 86 | r |
| 06A-67-23 | 166 | 676 | 2468 | 0.27 | 0.065678 | 0.000807 | 0.559318 | 0.011731 | 0.061264 | 0.000884 | 796 | 26 | 451 | 8 | 383 | 5 | 83 | r |
| *Sample 10a-8-1* | | | | | | | | | | | | | | | | | | |
| 10A-8-1-1 | 102 | 428 | 730 | 0.59 | 0.056560 | 0.000885 | 0.574300 | 0.007762 | 0.073821 | 0.000565 | 476 | 35 | 461 | 5 | 459 | 3 | 99 | |
| 10A-8-1-2 | 120 | 598 | 859 | 0.70 | 0.055799 | 0.001172 | 0.559192 | 0.012029 | 0.072341 | 0.000374 | 443 | 51 | 451 | 8 | 450 | 2 | 99 | |
| 10A-8-1-3 | 144 | 903 | 1172 | 0.77 | 0.055966 | 0.000727 | 0.550273 | 0.006872 | 0.071130 | 0.000298 | 450 | 30 | 445 | 5 | 443 | 2 | 99 | |
| 10A-8-1-4 | 112 | 381 | 820 | 0.47 | 0.055960 | 0.000895 | 0.549030 | 0.009187 | 0.070995 | 0.000383 | 450 | 35 | 444 | 6 | 442 | 2 | 99 | |
| 10A-8-1-5 | 74 | 365 | 425 | 0.86 | 0.065756 | 0.001673 | 0.614159 | 0.015675 | 0.067716 | 0.000621 | 798 | 53 | 486 | 10 | 422 | 4 | 85 | |
| 10A-8-1-6 | 161 | 1062 | 1239 | 0.86 | 0.061220 | 0.000833 | 0.569445 | 0.007676 | 0.067401 | 0.000223 | 656 | 30 | 458 | 5 | 420 | 1 | 91 | |
| 10A-8-1-7 | 119 | 1357 | 675 | 2.01 | 0.064462 | 0.001210 | 0.584901 | 0.011577 | 0.065743 | 0.000373 | 767 | 40 | 468 | 7 | 410 | 2 | 86 | |
| 10A-8-1-8 | 105 | 325 | 922 | 0.35 | 0.059588 | 0.001097 | 0.552555 | 0.009042 | 0.067648 | 0.000304 | 587 | 39 | 447 | 6 | 422 | 2 | 94 | |
| 10A-8-1-9 | 90 | 508 | 690 | 0.74 | 0.057434 | 0.001111 | 0.572317 | 0.010803 | 0.072352 | 0.000548 | 509 | 43 | 460 | 7 | 450 | 3 | 97 | |
| 10A-8-1-10 | 78 | 715 | 622 | 1.15 | 0.062719 | 0.002507 | 0.596297 | 0.022163 | 0.069086 | 0.000789 | 698 | 85 | 475 | 14 | 431 | 5 | 90 | |
| 10A-8-1-11 | 132 | 858 | 1126 | 0.76 | 0.060395 | 0.001259 | 0.557856 | 0.011064 | 0.067045 | 0.000428 | 617 | 44 | 450 | 7 | 418 | 3 | 92 | |
| 10A-8-1-12 | 107 | 2064 | 972 | 2.12 | 0.061107 | 0.001126 | 0.534757 | 0.009904 | 0.063383 | 0.000377 | 643 | 36 | 435 | 7 | 396 | 2 | 90 | |
| 10A-8-1-13 | 127 | 438 | 1184 | 0.37 | 0.058898 | 0.000791 | 0.537526 | 0.006759 | 0.066185 | 0.000236 | 565 | −5 | 437 | 4 | 413 | 1 | 94 | |
| *Sample 10a-7-1* | | | | | | | | | | | | | | | | | | |
| 10A-7-1-1 | 55 | 87 | 442 | 0.20 | 0.085990 | 0.002584 | 0.787770 | 0.035787 | 0.066027 | 0.000605 | 1339 | 58 | 590 | 20 | 412 | 4 | 64 | |
| 10A-7-1-2 | 140 | 322 | 1804 | 0.18 | 0.059157 | 0.001340 | 0.493541 | 0.018817 | 0.060039 | 0.000382 | 572 | 48 | 407 | 13 | 376 | 2 | 91 | |
| 10A-7-1-3 | 221 | 486 | 3057 | 0.16 | 0.060748 | 0.001788 | 0.511699 | 0.019868 | 0.060600 | 0.000436 | 632 | 64 | 420 | 13 | 379 | 3 | 89 | |
| 10A-7-1-4 | 528 | 759 | 7130 | 0.11 | 0.084306 | 0.000373 | 0.626058 | 0.015348 | 0.053461 | 0.000219 | 1300 | 5 | 494 | 10 | 336 | 1 | 61 | |
| 10A-7-1-5 | 110 | 245 | 1154 | 0.21 | 0.066092 | 0.001596 | 0.672303 | 0.024971 | 0.073146 | 0.000558 | 809 | 46 | 522 | 15 | 455 | 3 | 86 | |
| 10A-7-1-6 | 119 | 959 | 1091 | 0.88 | 0.062790 | 0.001524 | 0.582616 | 0.020883 | 0.066797 | 0.000453 | 702 | 52 | 466 | 13 | 417 | 3 | 88 | |
| 10A-7-1-7 | 144 | 972 | 1257 | 0.77 | 0.067776 | 0.000969 | 0.587818 | 0.017253 | 0.062344 | 0.000338 | 861 | 34 | 469 | 11 | 390 | 2 | 81 | |
| 10A-7-1-8 | 342 | 743 | 3762 | 0.20 | 0.084564 | 0.000824 | 0.709377 | 0.021832 | 0.060332 | 0.000989 | 1306 | 19 | 544 | 13 | 378 | 6 | 63 | |
| 10A-7-1-9 | 394 | 732 | 9001 | 0.08 | 0.078334 | 0.002511 | 0.364789 | 0.009593 | 0.034127 | 0.000741 | 1155 | 59 | 316 | 7 | 216 | 5 | 62 | |
| 10A-7-1-10 | 87 | 327 | 901 | 0.36 | 0.069378 | 0.001001 | 0.583922 | 0.016543 | 0.060781 | 0.000375 | 909 | 30 | 467 | 11 | 380 | 2 | 79 | |
| 10A-7-1-11 | 156 | 558 | 1375 | 0.41 | 0.075766 | 0.001291 | 0.636302 | 0.019995 | 0.060521 | 0.000373 | 1100 | 35 | 500 | 12 | 379 | 2 | 72 | |
| 10A-7-1-12 | 137 | 377 | 1702 | 0.22 | 0.061759 | 0.001041 | 0.503585 | 0.022066 | 0.058734 | 0.000685 | 665 | 37 | 414 | 15 | 368 | 4 | 88 | |

[a] Degree of concordance = ($^{238}U/^{206}Pb$ age × 100/$^{207}Pb/^{206}Pb$ age).

[b] lc = inherited cores; c = magmatic core; r = rim, domains distinguished on CL images.

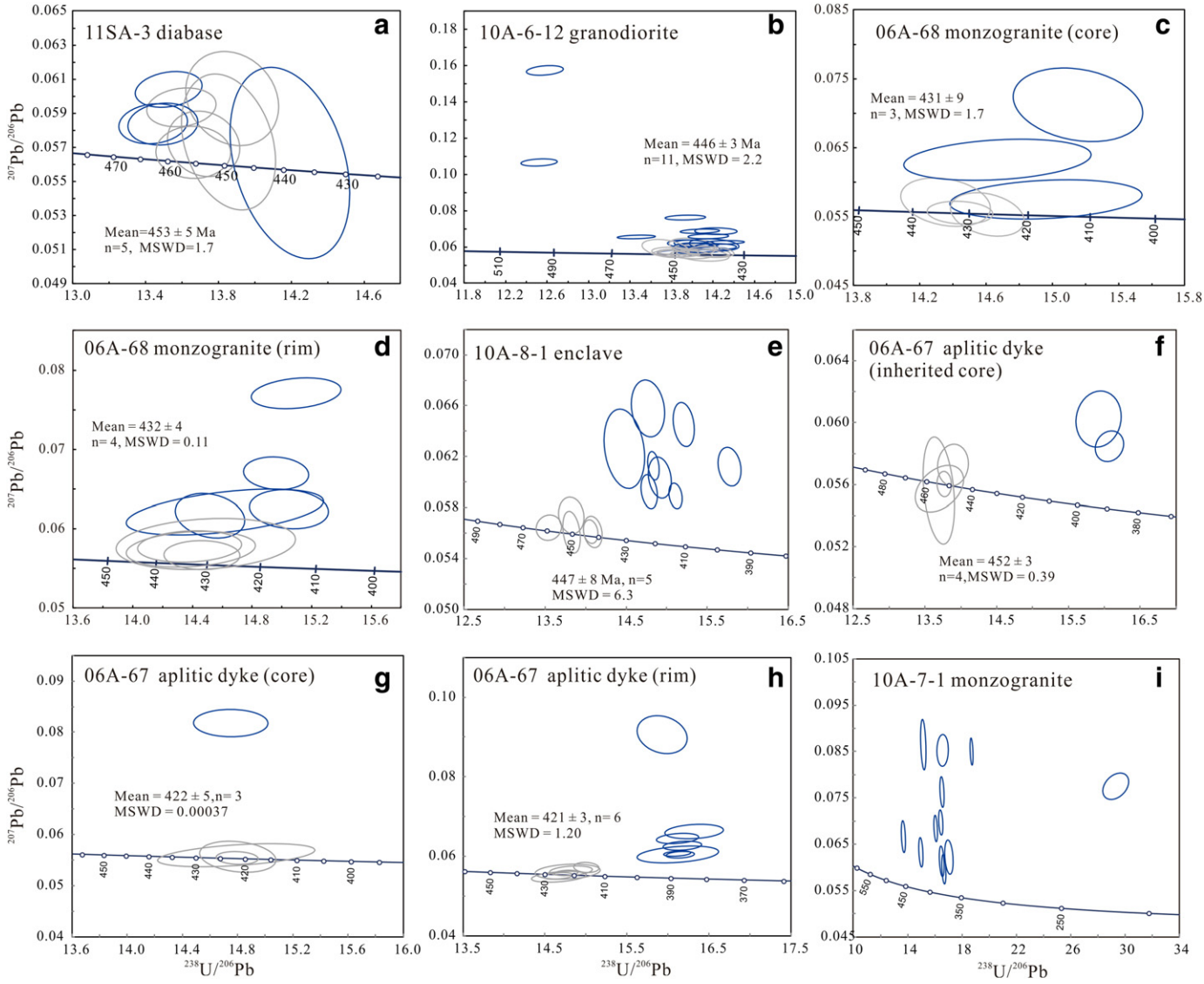


**Fig. 5.** Tera–Wasserburg concordia plots of U–Pb analyses of zircon from the South Altyn mafic and granitoids. Analytical uncertainties shown as 1σ. Gray-colored error ellipses show the calculated analyses for the mean $^{206}Pb/^{238}U$ ages.

Sample 10A-8-1 was collected from an enclave within the monzogranite of the YP. CL imaging shows that most of the crystals have a weak broad banded zoning (Fig. 4). Five concordant analyses yield a weighted mean $^{206}Pb/^{238}U$ age of 447 ± 8 Ma (Fig. 5e; MSWD = 6.3) that is interpreted as the crystallization age of the enclave.

Sample 06A-67 was collected from an aplitic dyke within the monzogranite of the YP. Zircons from this sample are characterized by gray CL inherited core surrounded by dark-gray fine-scale oscillatory zoning core and dark rim (Fig. 4). Most of the rims have very weak CL with no visible zoning (Fig. 4). In some cases, the boundary between core and rim can be difficult to distinguish. Four concordant core analyses yield a weighted mean $^{206}Pb/^{238}U$ age of 452 ± 3 Ma (Fig. 5f; MSWD = 0.39) that we interpret as inherited zircons in the aplitic dyke. Three concordant core analyses yield a weighted mean $^{206}Pb/^{238}U$ age of 422 ± 5 Ma (Fig. 5g; MSWD = 0.00037). Six concordant analyses from rims yield a weighted mean $^{206}Pb/^{238}U$ age of 421 ± 3 Ma (Fig. 5h; MSWD = 1.2). As both mantles and rims have similar ages, we interpret the crystallization age of the aplite as around 422–421 Ma.

Sample 10A-07-01 was collected from muscovite monzogranite of the BP. The analyzed zircons from this sample are discordant (Fig. 5i). However, based on field and chemical relationships, we believe this granite to be of Silurian–Devonian age.

### 6.2. Major and trace elements

#### 6.2.1. The mafic rocks

The main features of the studied mafic rocks are basalts and diabases ($SiO_2$ = 46.99–50.36 wt.%) (Fig. 6, Table 1). All samples are tholeiitic basalts. The REE chondrite-normalized plots and primitive mantle-normalized multi-element diagrams for basalts and diabases (Fig. 7a and b) are similar to that of enriched E-MORB. Moderate LREE/HREE fractionation ($La_N/Yb_N$ from 1.52 to 1.75) and elevated HREE abundance suggest that garnet was not an important residual source mineral. The primitive mantle-normalized compositions of the basalts and diabases show broadly parallel patterns, except for the Sr and Eu (Fig. 7b). The positive Sr and Eu anomalies in the diabases indicate plagioclase fractionation occurred in several samples. The trends of basalts and diabases (Fig. 7b) are broadly parallel to that of E-MORB for most elements, except for the Cs, Rb, Ba, K, and Sr where they are more enriched than E-MORB. The similarities to E-MORB element distributions, low to moderate LILE/HFSE ratios,

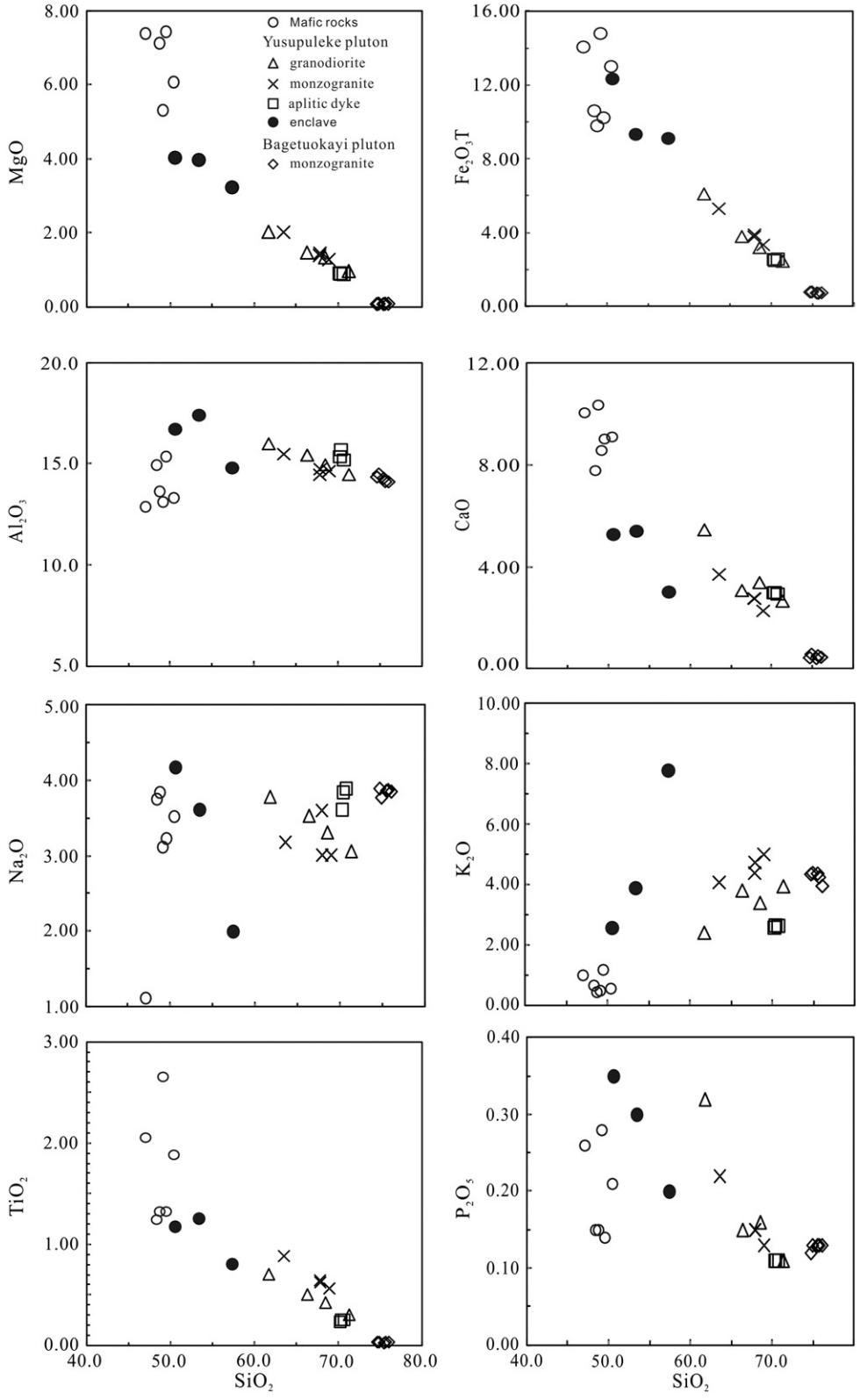


**Fig. 6.** $SiO_2$ v. major element plots for the South Altyn mafic and granitic rocks.

and absence of negative Nb and Ta anomalies imply that these mafic rocks did not form in a subduction setting (Fig. 7a and b). Furthermore, the spidergrams of basalts and diabases show the similarities to CFB element distributions (Fig. 7b). A more likely interpretation based on trace element patterns is that they originated in an extensional setting.

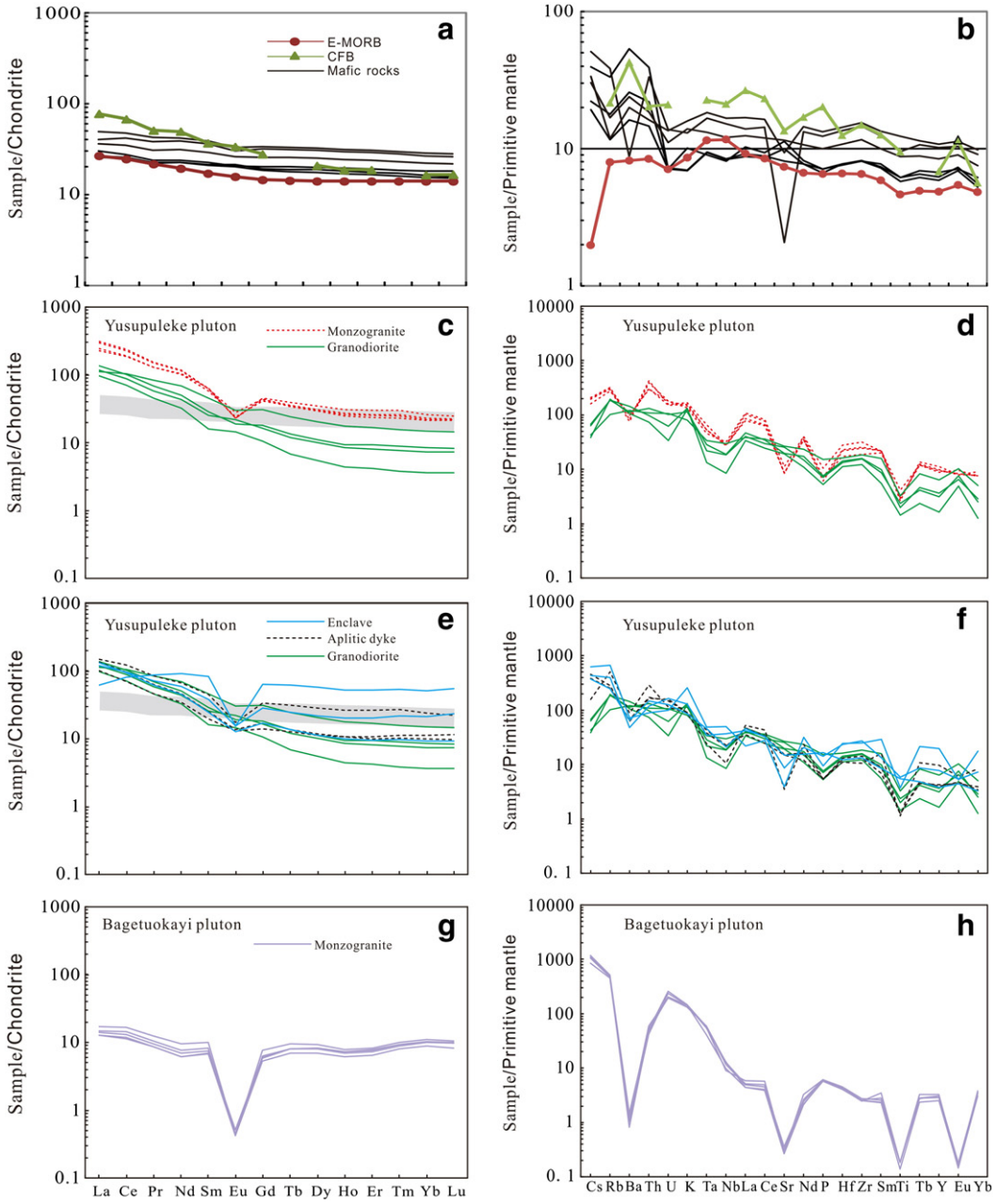


**Fig. 7.** REE chondrite normalized diagrams and primordial mantle normalized diagrams showing the mafic and granitic rocks of South Altyn. Normalizing chondrite and primordial mantle values are after Sun and McDonough (1989). E-MORB and OIB data are from Sun and McDonough (1989). Continental flood basalts (CFB) are from Wilson (1989). To aid in comparison between groupings, abundant samples from the mafic rocks are shown as a shaded field.

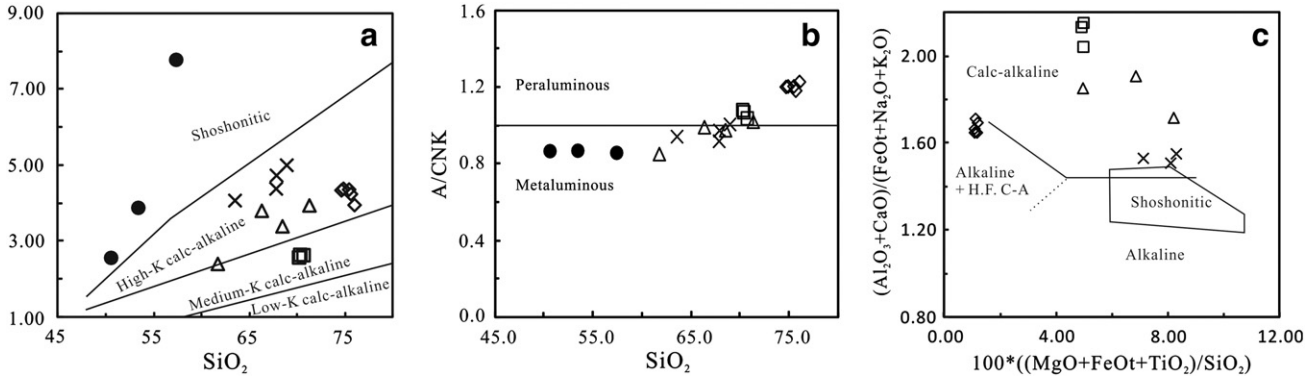


**Fig. 8.** Plot of South Altyn granitic rocks on: (a) $SiO_2$ vs. K2O classification diagram with the boundary lines after Le Maitre (1989) and Rickwood (1989). (b) $SiO_2$ versus A/CNK [ACNK = molar $Al_2O_3$ / ($CaO + Na_2O + K_2O$), Maniar and Piccoli (1989)]. (c) ($Al_2O_3 + CaO$) / ($FeOt + Na_2O + K_2O$) vs 100*(($MgO + FeOt + TiO_2$) / $SiO_2$) diagram (Liégeois et al., 1998) for the granites. Symbols as in Fig. 6.

*6.2.2. The Yusupuleke pluton*

Representative chemical compositions from the YP are given in Table 1. The samples from YP span a wide range of $SiO_2$ from about 50.5 to 71.3 wt.% (Table 1, Fig. 6) that includes granodiorites, monzogranites, monzodioritic enclaves and aplitic granite dykes. In the $K_2O$ versus $SiO_2$ diagram (Fig. 8a), granodiorites and monzogranites plot in the high K calc-alkaline field, monzodiorite enclaves plot in the shoshonitic field, and aplitic granite dykes plot as medium K calc-alkaline rocks. The YP granodiorites, monzogranites and its enclaves are metaluminous with A/CNK values clustering mostly around 0.9–1.0, whereas aplitic granites are all peraluminous with A/CNK values ranging from 1.0 to 1.1 (Fig. 8b). None of the samples yielded a

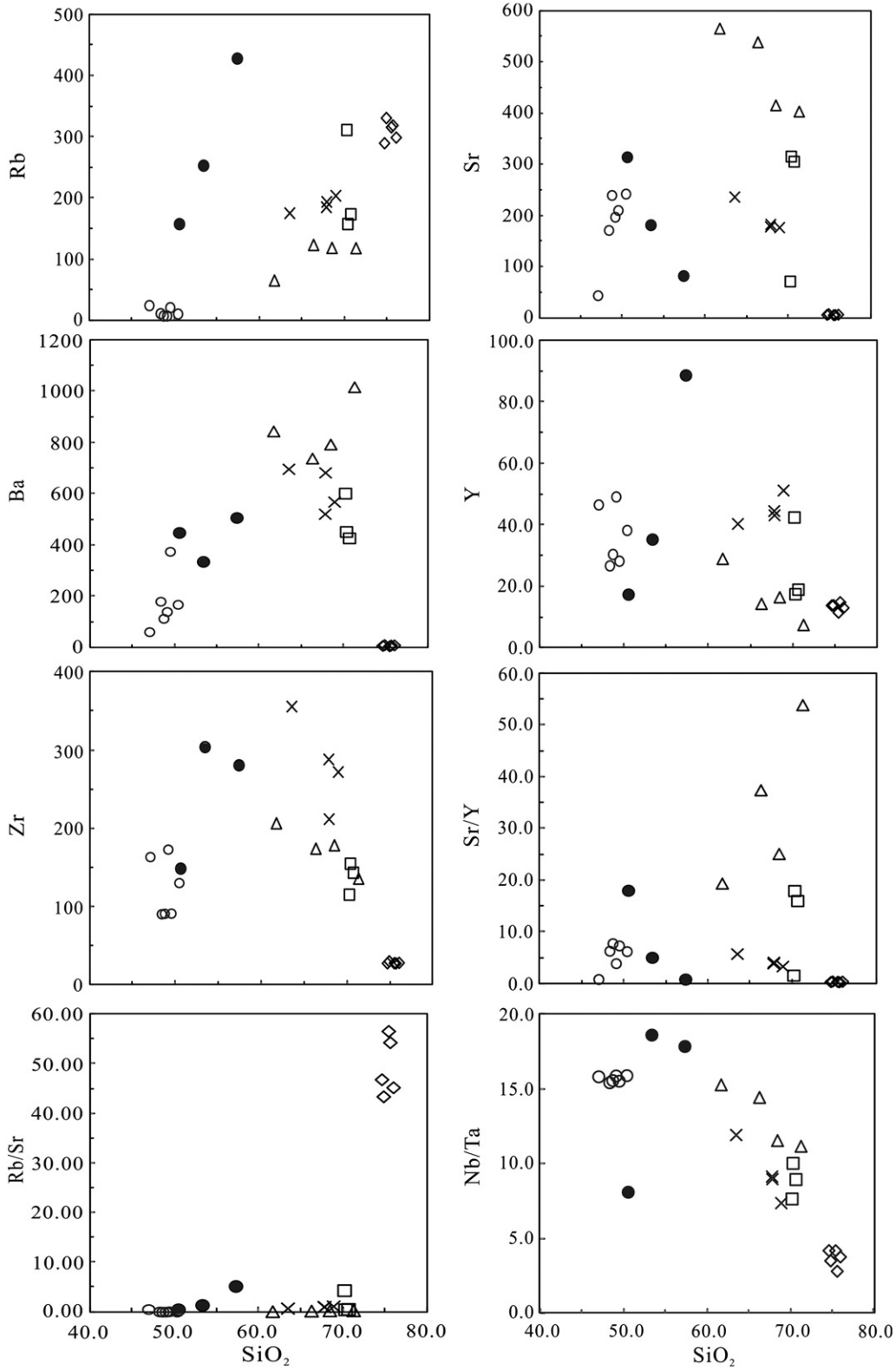


**Fig. 9.** $SiO_2$ v. trace element and element ratios plots for the South Altyn mafic and granitic rocks. Symbols as in Fig. 6.

NK/A > 1. Using the classification of Liégeois et al. (1998) these rocks from YP plot in the calc-alkaline field (Fig. 8c).

Rocks from the YP have moderate to high rare earth element contents (ΣREE = 94–327). The REE patterns are moderately fractionated. The $La_N/Yb_N$ ratios vary between 8 and 27 for granodiorites, between 9 and 15 for monzogranites and between 6 and 14 for aplitic granite and between 1 and 14 for the enclaves. The size of the negative Eu anomalies varies between 0.21 and 1.11 for YP rocks. There are no, or insignificant, negative Eu anomalies for the granodiorites (Fig. 7c). All are relatively enriched in the Large Ion Lithophile Elements (LILE—especially Cs, Rb, Th and K) and the LREE, with negative Ta, Nb and Ti anomalies. Trace elements show strong variations between the different rock types. Granodiorites show very small (to insignificant) negative Ba and Sr anomalies (Fig. 7d), whereas other magmatic products are generally more HREE-enriched with pronounced negative Ba, Sr, P, Eu and Ti anomalies compared to the granodiorites. The REE patterns of aplitic dykes and enclaves are subparallel and are quite similar to those observed in the granodiorites. The enclaves also exhibit significant variations in several trace element contents (Fig. 7e), that may be controlled by the presence of various accessory minerals incorporated during the process of magma mixing (Wang et al., 2008).

#### 6.2.3. The Bagetuokayi pluton

The BP monzogranites have $SiO_2$ contents of 74.6–76.0 wt.%. The rocks plot as high-K calc-alkaline series (Fig. 8a) with correspondingly high $K_2O$ content. They are strongly peraluminous with A/CNK values around 1.2 (Table 1; Fig. 8b). These granitic rocks are all alkali-rich, with all samples plotting in the alkaline and highly fractionated calc-alkaline fields (Fig. 8c). In comparison to the rocks of the YP, the BG tend to have lower contents of $Al_2O_3$, MgO, $TiO_2$, CaO, Ba, Sr, Y and Zr (Figs. 6 and 9). The low contents of Sr and Ba result in high Rb/Sr and low Sr/Y ratios (Fig. 9).

The REE patterns of BP monzogranites differ significantly from the REE patterns of the YP rocks. They show rather flat patterns ($La_N/Yb_N$ = 1.25–1.53) and low rare earth element contents (ΣREE = 21–30) with pronouncedly negative Eu anomalies ($Eu/Eu^*$ = 0.02; Fig. 7g). Primitive mantle normalized trace element patterns for the BP monzogranites are characteristics of WPG (Whalen et al., 2006), with more pronounced negative Ba, Sr, P, Eu and Ti anomalies than YP samples (Fig. 7h). The BP granites have high Ga/Al ratios falling within the A-type granite field of Whalen et al. (1987).

## 7. Discussion

### 7.1. Possible source for various magmas

#### 7.1.1. Mafic magmas

The mafic rocks have lower Mg# (45.5–65.0) and Ni (27.8–172.7 ppm) and Cr (11.0–393.4) contents than those of primary melt (e.g. Frey et al., 1978), reflecting removal of Mg, Ni and Cr via olivine and pyroxene fractionation (e.g. Dixon and Batiza, 1979). Mafic magmas that undergo crustal contamination are expected to display Nb, Ti, P depletion combined with enrichment in Th (Taylor and McLennan, 1995). Samples in this study lack negative Ta, Nb, Ti and P anomalies and show low Th on primitive mantle normalized plots (Fig. 7b) indicating an ascent of melt with no significant crustal contamination. A Th/Yb vs. Nb/Yb plot (Fig. 10a) also indicates that the mafic magmas were not affected by any significant contamination due to the lack of a marked shift towards higher Th/Yb ratios and displacement from the mantle array (e.g. Aldanmaz et al., 2006). In the Zr/Y vs. Nb/Y diagram (Fig. 10b), magmas for these rocks resemble those of PM transitional to OIBs and the data plot above the enrichment-depletion tie-line (ΔNb = 0 line). These observations suggest that the rocks were generated from variably enriched mantle regions (e.g. Condie, 2005). The enrichment of the non-arc type mafic rocks in LILE (Rb, Cs), as well as in REE and other HFSE (Fig. 7b) can be related to an asthenospheric effect combined with melting of the subduction metasomatized subcontinental lithospheric mantle (SCLM; Whalen et al., 2006). Partial melting of SCLM to produce LILE enriched magmas depends on both timing of metasomatism plus metasomatizing fluid composition (Whalen et al., 2006).

#### 7.1.2. Yusupuleke pluton

*7.1.2.1. Granodiorites.* There are two possible processes thought to be responsible for the origin of granodiorites. These are through partial melting of the continental crust or via fractionation of coeval mafic magma. In our case, the granodiorites are characterized by high Mg#, the least fractionated REE pattern lacking Eu anomaly, as well as high Sr contents and low Rb/Sr ratios (Fig. 9). This makes a fractional crystallization origin a less likely explanation. In addition, the fractionation is less probable due to the lack of intermediate composition rocks in the YP. Thus, it seems more likely that the granodiorites were formed by partial melting of crustal source rocks. The composition of this crustal source region can also be gleaned from the chemical composition of the granodiorites. The

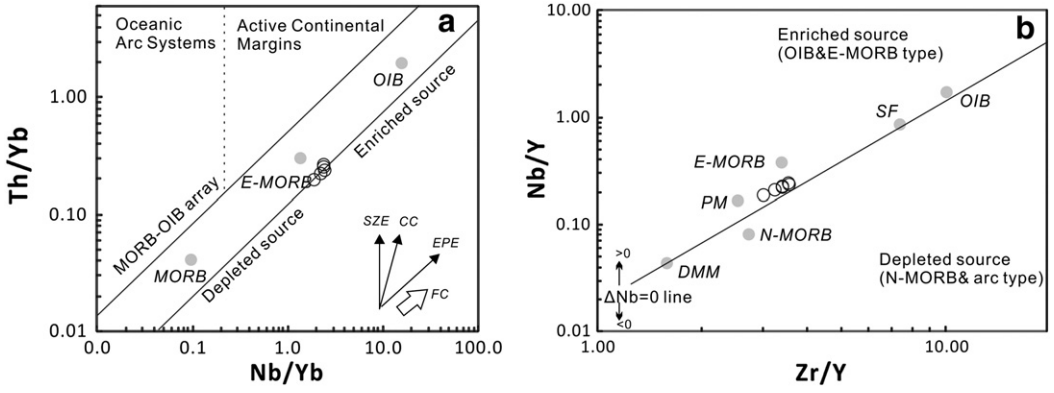


**Fig. 10.** (a) Th/Yb vs. Nb/Yb diagram from Pearce et al. (1995). (b). Nb/Y vs. Zr/Y diagram for the BOM. The ΔNb = 0 line separates enriched (ΔNb > 0) from depleted (ΔNb < 0) sources (after Condie, 2005). The studied samples plot close to values of E-MORB. SZE: subduction zone enrichment, CC: continental contamination, WPE: within-plate enrichment, FC: fractional crystallization.

lack of Eu and Sr anomalies argue against fractionation of plagioclase. On the other hand, the high Sr (403–565 ppm), moderate to high Sr/Y (19.5–54.0) and fractionated REE patterns (high La/Yb ratios) together with the overall low abundances of Y (7.5–29.0 ppm) and HREE require the presence of garnet or amphibole as a fractionating or residual phase. Thus, an amphibole-bearing residue for the granodiorites is consistent with the high $Al_2O_3$ concentration and low Rb/Sr and K/Rb ratios (e.g. Petford and Atherton, 1996). Experimental evidence also suggests that the melts have a residual mineral assemblage of clinopyroxene, amphibole, plagioclase and garnet at >16 kbar and a plagioclase-absent, garnet-bearing amphibolite, granulite or eclogite at 22–30 kbar (Rapp and Watson, 1995). The observed small variation in the Sr/Y (19–54) and Dy/Yb ratios (2.0–2.2) for the YP granodiorites indicate that the melts were generated from a similar source by variable degrees of crustal partial melting where the source has varying proportions of residual garnet and amphibole. These features indicate that the source rock of the granodiorites melts could have formed from garnet amphibolite sources at pressures between 16 and 22 kbar in the lower crust. The melts might be in equilibrium with garnet-bearing amphibolite or granulite source in the lower crust (e.g. Rapp and Watson, 1995). Application of the saturation equations for Zr of Watson and Harrison (1983) yielded temperature ranges of 764–782 °C for the I-type granodiorites.

*7.1.2.2. Monzogranites.* The monzogranites have an overall composition similar to that of granodiorite (Fig. 7). However, the monzogranites were formed ~30 Ma after intrusion of the granodiorites. Given the age relationships, the monzogranites cannot represent fractionation products of the granodiorite melt. The monzogranites have low Rb/Sr ratios and moderate Sr, Sr/Y, $CaO/Na_2O$ (0.8–1.2) and negative Eu anomalies. Those features indicate that they have undergone weak fractional crystallization from a source that lacked garnet but contained both amphibole and plagioclase in the residue (e.g. Petford and Atherton, 1996). This is distinct from the source of the granodiorites. The negative anomalies of Ba, Sr, P and Ti in the spidergrams (Fig. 7) display the same features. Such magmas may be generated by melting of intermediate metaigneous rock within the middle or the lower crust (Jung and Pfänder, 2007). The calculated zircon saturation temperatures ($T_{Zr}$) of the YP monzogranites yield saturation temperatures of 796–831 °C (Table 1).

*7.1.2.3. Magmatic enclaves.* Enclaves have low $SiO_2$ (50.5–57.3 wt.%) and weak negative Eu anomalies, indicating a mafic source. Enclaves show chemical affinities with shoshonitic magmas (e.g., high $K_2O$, P, Rb, Sr, Ba, LREE, high but variable $Al_2O_3$ (14.8–17.4 wt.%; Morrison, 1980)). Previous studies suggested that shoshonitic magmas originated either by partial melting of the subcontinental lithospheric mantle or asthenospheric mantle (e.g. Guo et al., 2006; Miller et al., 1999; Williams et al., 2004). Shoshonitic magmas share a LILE-enriched metasomatized mantle origin (e.g. Conceição and Green, 2004; Murphy, 2013), in which pargasite is the dominant phase in controlling melt compositions and fertility (e.g. Conceição and Green, 2004). Enclaves have higher Nb/Ta ratios (17.9–18.6) except sample 06A-69. Sample 06A-69 appears to be a primitive mantle rock (Nb/Ta = 17.5 ± 2.0, Rudnick and Gao, 2003). The weak negative Ba, Sr and Ti contents in enclaves can be related to limited fractionation of the plagioclase and/or K-feldspar and Ti-bearing minerals in the course of enclave development. Thus, the enrichments P and HFSE (Nb, Zr, Hf) observed in the enclaves would seemingly indicate that the more mafic phases were produced by partial melting of highly enriched mantle. In contrast to the highly enriched mantle source model, our enclaves contain enriched LILE (notably K, Rb, Cs and Sr) and LREE, and show variable major element contents and REE patterns (Fig. 6). These characteristics correspond to a chemical/metasomatic exchange between the mafic magma and granitic magma during cooling (Waight et al., 2001), two-component mixing in different proportions (Barbarin, 2005) or fractional crystallization of a hybrid parental magma (Collins et al., 2006). We argue that the most parsimonious explanation for the origin of the mafic enclaves is that they represent hybrid magmas of bulk intermediate composition. This is supported by a linear trend between basalts at 50 wt.% $SiO_2$ and the most primitive enclave-free granitoids at 63 wt.% $SiO_2$ (Fig. 7). The hybrid nature of microgranular enclaves is also confirmed by the presence of disequilibrium features such as large/oriented crystals of alkali feldspar xenocrysts, feldspar-sphene ocelli and long prismatic apatite within the enclaves (Wang et al., 2008).

*7.1.2.4. Aplitic dykes.* Aplitic dykes have similar features as REE, trace element patterns (Fig. 7e) to those of granodiorites with the exception that the aplites have more negative Sr anomalies and higher $SiO_2$ contents. The aplites have low Rb/Sr and moderate Sr, Sr/Y (Fig. 9) and small negative Eu anomalies. The chemistry is inconsistent with fractional crystallization models, but fits with a partial melting origin with magmas generated from the granodiorites in the region. A partial melting origin is supported by the relatively high Mg-number (43.1–45.3). The negative Nb, P and Ti anomalies may reflect the characteristics of a magma source. Low Nb/Ta ratios (7.66:10.04) in the aplites are similar to those of lower crust (8.3, Rudnick and Gao, 2003) and a magma source with amphibole and rutile (~9.00, Dostal and Chatterjee, 2000). Zircons from the aplite show inherited ages (ca. 451 Ma) that are nearly identical to those of the granodiorites (ca. 446 Ma) supporting a genetic connection between the two bodies. The calculated zircon saturation temperatures ($T_{Zr}$) of the YP aplitic granites range between 759 and 782 °C (Table 1). Because the aplitic dykes contain abundant inherited zircons, the temperature estimates presented here are considered maxima.

*7.1.3. Bagetuokayi pluton*

BP monzogranites are strongly peraluminous granites with A/CNK values around 1.2. $CaO/Na_2O$ ratios of granites are controlled by the plagioclase/clay ratio of the source: strongly peraluminous granite melts produced from plagioclase-poor, clay-rich sources will tend to have lower $CaO/Na_2O$ ratios than melts derived from sources which are plagioclase-rich and clay-poor (Sylvester, 1998). BP monzogranites are characterized by low $CaO/Na_2O$ ratios (0.11–0.16 < 0.3), indicating a metapelitic source (e.g., Sylvester, 1998). This conclusion is also supported by the relationships between Rb/Sr vs. Rb/Ba (Fig. 11; Sylvester, 1998). The Rb, Sr and Ba in granitic systems are contained in mica and feldspar (e.g., Harris and Inger, 1992). The presence of pronounced negative Eu anomalies and high Rb/Sr and Rb/Ba is compatible with anatexis of a feldspar-rich source. The observed increase of Rb/Sr and Rb/Ba in the melt relative to the metapelite is simply a function of the amount of residual plagioclase and K-feldspar (e.g., Sylvester, 1998). BP monzogranites yield Zr saturation temperatures ranging between 665 and 672 °C.

*7.2. Tectonic implications*

*7.2.1. Timing framework of a post-collisional setting*

The new U–Pb zircon geochronological data acquired on a selection of samples provide more detailed constraints on the timing and tectonic setting for these magmatic suites. The main magmatic pulse took place at 485–445 Ma, leading to formation of the high-K calc-alkaline granitoids both in the Qimantagh and South Altyn along with the emplacement of ~465–445 Ma mafic–ultramafic intrusions along the Altyn Tagh fault, and eruption of bimodal volcanic rocks in the Qimantagh. The geochronological data also indicate that emplacement of the post-collisional suites overlap with the retrograde HP granulite-facies metamorphism at ~455 Ma and ductile shearing within the South Altyn fault (Fig. 12).

A second magmatic pulse at 440–380 Ma emplaced mafic dykes and A-type granites along the southern side of the Altyn Tagh fault (Fig. 1c). The A-type granite contains two facies that were emplaced between ca. 440 and 420 Ma and ca. 420–380 Ma. In this study, the first sub-phase

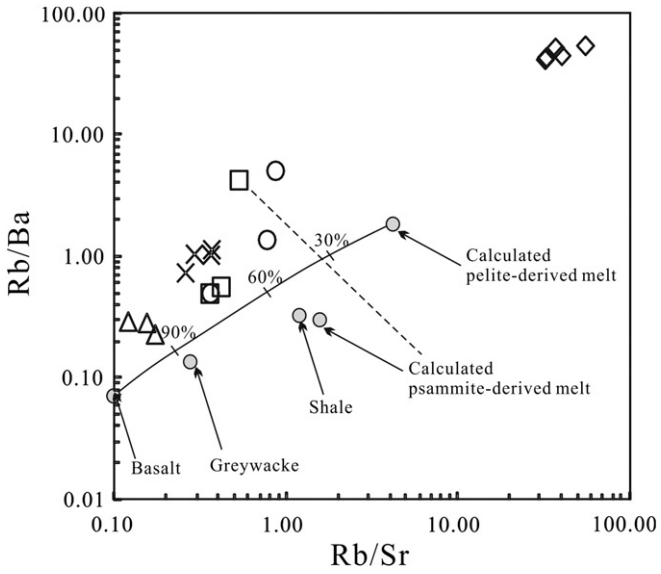


**Fig. 11.** Rb/Sr vs. Rb/Ba diagram (Sylvester, 1998). Symbols as in Fig. 6.

(440–420 Ma) is related to calc-alkaline monzogranites and aplitic dykes of the YP, and the second sub-phase (420–380 Ma) is represented by the alkaline series of BP and the Tula granitic pluton. The second sub-phase is coeval with: i) mafic dyke swarms from the Qimantagh; ii) a foliation-parallel leucosome from migmatite of South Altyn formed at 417 Ma; and iii) a ductile deformation phase of South Altyn and Baiganhu faults (Fig. 12). The metamorphic peak in the South Altyn predates the main phases of ductile deformation (Fig. 12). Post-collisional igneous rocks are exposed along several faults trending NE–SW and NW–SE in the Qimantagh and also NE–SW and E–W in the South Altyn. Therefore, emplacement of the post-collisional igneous suites may be controlled by these structural lineaments. U–Pb zircon geochronology of Paleozoic granitoids and mafic igneous rocks of the Qimantagh–South Altyn reveals that most of the magmatism is either coeval with, or post-dates, ductile deformation in the region (Fig. 12).

*7.2.2. Implications for the East Kunlun–Altyn Tagh continental collision*

Numerous studies in the Altyn Tagh and East Kunlun regions have failed to discern the Paleozoic evolution of these two regions. In many cases, this is due to older interpretations wherein the two regions were thought to represent distinct domains that were juxtaposed by sinistral slip along the Altyn Tagh fault during the Mesozoic–Cenozoic Indo-Asian collision (e.g. Cowgill et al., 2003; Molnar and Tapponier, 1975; Peltzer and Tapponnier, 1988; Ritts and Biffi, 2000; Xu et al., 1999; Yang et al., 2003; Yin et al., 2002). Previous estimates of total offset along the Altyn Tagh fault range from 280 to 500 km. New research suggests that both the peak and retrograde metamorphic ages for the South Altyn eclogite are distinct from the North Qaidam HP/UHP eclogites. Thus, the South Altyn and North Qaidam eclogites do not belong to the same HP/UHP metamorphic terrain (Liu et al., 2012). The Altyn Tagh fault was likely diachronous. It contains 623 Ma Dimulalike basic volcanic breccias (Yang et al., 2012), ca. 500 Ma ophiolite mélange (Li et al., 2009; Liu et al., 1998) and ca. 445–467 Ma mafic–ultramafic layered intrusions (Ma et al., 2011; this study). Thus, it is likely that the Altyn Tagh fault was once a suture zone. As mentioned above (see Section 2), vast high-grade metamorphic rocks of Altyn Complex indicate an early Paleozoic age for the subduction–collision belt in South Altyn. Liu et al. (2013) suggested that northward subduction led to the continent–continent collision. The main collision, corresponding to crustal thickening and to the peak eclogite-facies metamorphism, occurred ca. 500 Ma. Cao et al. (2010) and Yang et al. (2012) consider that part of the 462–451 Ma plutons intrusive in the South Altyn formed in a post-collisional setting. Geochronological and geochemical data from this study suggest that the numerous granitoids and mafic rocks from the Qimantagh–South Altyn intruded between 485 and 380 Ma in either a post-collisional or within-plate regime (Fig. 12). The space–time relation in the generation of the metamorphism–magmatism on both sides of the Altyn Tagh fault suggests that these rocks record the transition from continental collision to post-collisional and post-orogenic settings between the East Kunlun and Altyn Tagh.

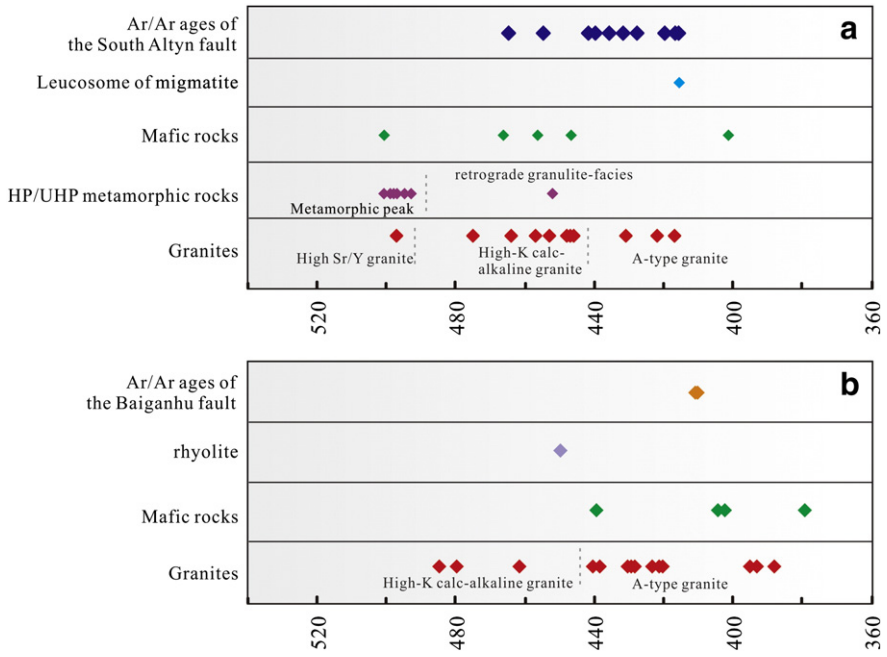


**Fig. 12.** Diagram showing the age variation and time relations of deformation and metamorphic processes and magma generation and intrusion in the South Altyn (a) and Qimantagh (b). See the details described in the main text.

*7.2.3. Petrogenetic model*

The results of this study are crucial in delineating geochemical variations and magmatic processes in the region. According to U–Pb geochronological data, the Qimantagh–South Altyn post-collisional to postorogenic magmatism occurred over a 100 million year time span (Fig. 12). This time interval is much longer than the maximum residence times of shallow silicic magma chambers (e.g., Halliday et al., 1989). Variations in the geochemistry of the igneous rocks outlined in this paper support differing source regions and mechanisms for melt generation at discrete time intervals.

We propose that the ~500 Ma collisional orogenesis led to significant crustal thickening and shortening leading to the development of the HP/UHP and HP/UHT metamorphic rocks in South Altyn. Pressure–temperature estimates for this metamorphism is up to 2.8 GPa at 720–870 °C for the UHP eclogite-facies metamorphism. This would indicate crustal subduction to at least 80 km at 500 Ma (Liu et al., 2012). The ca. 500 Ma zircons in felsic granulite give temperatures of 870–1050 °C (Zhang et al., 2005). These data indicate accretion and subsequent collision in this region (e.g., Zhang et al., 2010). High Sr/Y adakites dated to ~500 Ma are products of partial melting of a thickened mafic lower crust in the South Altyn during mantle unrooting (e.g., Marotta et al., 1998) or the initial phases of orogenic collapse (e.g., Dewey, 1988). Thermo-mechanical numerical models demonstrate that as crust thickens during shortening, the lowermost crust may undergo metamorphic eclogitization and a concomitant increase in density (Krystopowicz and Currie, 2013). The eclogitic crustal root is then prone to gravitational removal through delamination (Kay and Kay, 1993). Granulite facies HP metamorphism took place at temperatures between 625 and 790 °C at pressures between 1.42 and 1.52 GPa at 455 ± 2 Ma. Amphibolite facies metamorphism occurred at temperatures between 600 and 730 °C and 0.99–1.17 GPa and thus preserves a history of exhumation through various crustal depths in the South Altyn (Liu et al., 2012). The exhumation stages are also supported by the retrograde metamorphic transition from Grt peridotite to Amp–Grt peridotite to Spl peridotite of the Yinggelesayi UHPM peridotite from South Altyn (Wang et al., 2011). The multistage exhumation may be related to uplift that was a result of the removal of a thickened crust in this region.

Convective removal of a conductive thermal boundary layer can result in the transition from crustal thickening to crustal thinning as the lowermost lithosphere is detached from the crust and founders in the less dense asthenospheric mantle (Bird, 1979; Davies and von Blankenburg, 1995; Houseman et al., 1981). These models all indicate the thickened lithospheric root is replaced by asthenospheric mantle.

Post-collisional magmatism described in this study and others (e.g., Bonin, 2004; Liégeois, 1998; Oyhantçabal et al., 2007; Turner et al., 1999) suggests that an asthenosphere-derived signature can indicate extensional collapse and thinning of the mantle lithosphere. Available geochemical data for mafic magmatism in the South Altyn region indicate an enriched subcontinental lithospheric mantle (SCLM) that resulted in the emplacement of tholeiitic and shoshonitic magmas from enriched mantle sources at 457–467 Ma, along with the cumulate rocks of the Yuemakeqi layered series. Additionally, the emplacement of long-lasting (10 Ma) mantle-derived magmas caused partial melting of the lower crust and produced the YP high-K calc-alkaline granodiorites at 446 Ma. Felsic rocks incorporate a mafic lower crustal component. It is likely that emplacement of mafic and granitic magmas were controlled by E–W trending shear zones resulting from the thermal weakening of the crust. We interpret these observations to reflect lithospheric thinning that facilitated asthenospheric mantle upwelling and concomitant melting of the lower crust. These processes gave rise to the mafic rocks and high Sr/Y granitoids of the South Altyn. Extension and thinning of the continental crust led to disappearance of the adakitic signature. At this stage, Ordovician–Silurian rift basins developed in the Qimantagh. These basins contain shallow and deep-water clastics, carbonates and bimodal volcanics with back-arc affinities (Jiang et al., 1992; Wang et al., 2010, 2012).

At the end of the post-collisional stage, rapid unroofing by isostasy is accompanied by hot asthenospheric upwelling and magmatic underplating. As a result of upwelling and underplating, the continental lithosphere is thinned (Bonin, 2004; Oyhantçabal et al., 2007). At this stage, A-type granites formed by melting of intermediate metaigneous rock within the middle or the lower crust with amphibole and plagioclase in the residue. This interpretation is supported by the melting experiments of hornblende and biotite bearing granitoids (Patiño Douce, 1997). Partial melting of pre-existing crust is produced by the successive emplacement of hot, mantle-derived magma in "deep crustal hot zones" (Annen et al., 2006). In this model, mafic sills are emplaced in the lower crust at the mantle-crust interface or at higher levels in the crust. After an incubation period, melts are generated by incomplete crystallization of the mafic magma and by partial melting of the pre-existing crust. The magmas may move directly to their final emplacement level as plutonic bodies, form shallow magma chambers, or stall and differentiate in one or more intermediate magma chambers (Solano et al., 2012). In Qimantagh–South Altyn, the next magmatic pulse at 440–380 Ma corresponds to A-type granite, when thickness of both lithospheric mantle and crust decreased. At ca. 421 Ma, melting of the older (ca. 446 Ma) granodiorites resulted in the intrusion of aplitic dykes into the monzogranite. The aplitic dyke episode is broadly associated with the development of a foliation-parallel leucosome migmatite at 417 Ma (Fig. 12) and related to the activation of major shear zones and crustal anatexis (Fig. 12). The Yusuputage batholith was emplaced over a 40 million year long period and thus resulted from a discontinuous magma flux into the reservoir.

Asthenospheric upwelling resulted in thermal erosion of the lithospheric mantle and, ultimately, to its delamination between neighboring shear zones (Liegeois et al., 1998). Dehydration of the thinning lithosphere results in an evolutionary shift from high-K calc-alkaline to alkaline magmatic suites in a short period of time (Bonin, 2004). In the Qimantagh–South Altyn regions, delamination caused an increase in extensional alkaline A-type granites and mafic dyke swarms (380 to ~400 Ma). This magmatic activity was contemporaneous with the development of late Devonian red molasse deposits derived from the volcanic products in the eastern part of East Kunlun.

Extensional collapse in the East Kunlun–Altyn Tagh encompasses the post-collisional to postorogenic magmatic suites. This phase includes the exhumation of HP/UHP metamorphic rocks from the base of the crust along with the development of extensional basins, thrusting and strike-slip faulting that accompany crustal thinning (e.g., Andersen and Jamtvet, 1990; Dewey, 1988; Frisch and Kuhlemann, 2000; Platt and Vissers, 1989; Turner, 1992; Turner et al., 1999). We suggest that orogenic collapse occurred by the removal of the thickened lithospheric root beneath the East Kunlun–Altyn Tagh collisional ridge during early Paleozoic.

## 8. Conclusions

Early Paleozoic magmatism in the Qimantagh–South Altyn occurred in post-collisional and postorogenic settings coinciding with the transition from crustal thickening to crustal thinning during the extensional collapse of an orogenic belt. The main period of felsic and mafic magma took place between 485 Ma and 380 Ma in the Qimantagh–South Altyn, accompanied with extensional deformation, exhumation of HP/UHP metamorphic rocks and crustal anatexis. Magmatic activity started with the emplacement of 485–445 Ma high-K calc-alkaline granitoids, metasomatization of subcontinental lithospheric mantle leading to the development of 467–445 Ma mafic-ultramafic magmas, followed by 440–420 Ma A-type granite emplacement and finally, the development of 400–380 Ma alkaline granite and mafic dykes. The HP/UHP metamorphic rocks, the post-collisional to postorogenic magmatic suites and extensional basins distributed within the Qimantagh–South Altyn correspond to collisional orogenesis and extensional collapse along the East Kunlun–Altyn Tagh during early Paleozoic.

## Acknowledgments

This work is supported by the National Natural Science Foundation of China (Grant Nos. 40902022, 40972128, 41272089), the Natural Science Foundation of Shaanxi Province, China (Grant No. 2010JM5007), the China Geological Survey (No. 1212010610102), and the Science and Technology Planning Project of Shaanxi Province, China (Grant No. 2014KJXX-19). We are grateful to Drs. Xiaoming Liu, Jianqi Wang, Ye Liu, Hujun Gong, and Chunrong Diwu for their help with chemical and isotopic analyses at the Northwest University, China. Detailed reviews from two anonymous reviewers helped in greatly improving this paper and are gratefully acknowledged. Dr. Nelson Eby is thanked for his comments and editorial handling of the manuscript.

## References

Aldanmaz, E., Köprüba, N., Gürer, Ö.F., Kaymakç, N., Gourgaud, A., 2006. Geochemical constraints on the Cenozoic, OIB-type alkaline volcanic rocks of NW Turkey: implications for mantle sources and melting processes. Lithos 86, 50–76.

Andersen, T.B., Jamtvet, B., 1990. Uplift of deep crust during orogenic extensional collapse: a model based on field studies in the Sogn-Sunnfjord region of W. Norway. Tectonics 9, 1097–1111.

Annen, C., Blundy, J.D., Sparks, R.S.J., 2006. The genesis of intermediate and silicic magmas in deep crustal hot zones. Journal of Petrology 47, 505–539.

Bao, G.P., Wang, G.P., Liu, R., Han, H.C., 2013. Kayakedengtage area two basic dike rocks geochemistry and significance. Northwestern Geology 46 (2), 37–43 (in Chinese with English abstract).

Barbarin, B., 2005. Mafic magmatic enclaves and mafic rocks associated with some granitoids of the central Sierra Nevada batholith, California: nature, origin, and relations with the hosts. Lithos 80, 155–177.

Bian, Q.T., Li, D.H., Pospelov, I., Yin, L.-M., Li, H.S., Zhao, D.S., Chang, C.F., Luo, X.Q., Gao, S.L., Astrakhantsev, O., Chamov, N., 2004. Age, geochemistry and tectonic setting of Buqingshan ophiolites, North Qinghai–Tibet Plateau, China. Journal of Asian Earth Sciences 23, 577–596.

Bird, P., 1979. Continental delamination and the Colorado Plateau. Journal of Geophysical Research: Solid Earth 84, 7561–7571.

Bonin, B., 2004. Do coeval mafic and felsic magmas in post-collisional to within-plate regimes necessarily imply two contrasting, mantle and crustal, sources? A review. Lithos 78, 1–24.

Cao, Y.T., Liu, L., Wang, C., Chen, D.L., Zhang, A.D., 2009. P–T path of Early Paleozoic pelitic high-pressure granulite from Danshuiquan area in Altyn Tagh. Acta Petrologica Sinica 25, 2260–2270 (in Chinese with English abstract).

Cao, Y.T., Liu, L., Wang, C., Yang, W.Q., Zhu, X.H., 2010. Geochemical, zircon U–Pb dating and Hf isotope compositions studies for Tatelekebulake granite in South Altyn Tagh. Acta Petrologica Sinica 26, 3259–3271 (in Chinese with English abstract).

Cao, Y.T., Liu, L., Wang, C., Kang, L., Yang, W.Q., Liang, S., Liao, X.Y., Wang, Y.W., 2013. Determination and implication of the HP pelitic granulite from the Munabulake area in the South Altyn Tagh. Acta Petrologica Sinica 29 (5), 1727–1739 (in Chinese with English abstract).

Che, Z., Liu, L., Luo, J., 1995. The discovery and occurrence of high-pressure metamorphic rocks from Altyn Mountain area, Xinjiang Autonomous Region. Chinese Science Bulletin 40, 1298–1300 (in Chinese with English abstract).

Chen, H.W., Luo, Z.H., Mo, X.X., Zhang, X.T., Wang, J., Wang, B.Z., 2006. SHRIMP ages of Kayakedengtage complex in the East Kunlun Mountains and their geological implications. Acta Petrologica et Mineralogica 25 (1), 25–32 (in Chinese with English abstract).

Clemens, J.D., Darbyshire, D.P.F., Flinders, J., 2009. Sources of post-orogenic calcalkaline magmas: the Arrochar and Garabal Hill–Glen Fyne complexes, Scotland. Lithos 112, 524–542.

Collins, W.J., Wiebe, R.A., Healy, B., Richards, S.W., 2006. Replenishment, crystal accumulation and floor aggradation in the megacrystic Kameruka Suite, Australia. Journal of Petrology 47, 2073–2104.

Conceição, R.V., Green, D.H., 2004. Derivation of potassic (shoshonitic) magmas by decompressing decompressing melting of phlogopite + pargasite lherzolite. Lithos 72, 209–229.

Condie, K.C., 2005. High field strength element ratios in Archean basalts: a window to evolving sources of mantle plumes? Lithos 79, 491–504.

Coney, P.J., Harms, T.A., 1984. Cordilleran metamorphic core complexes: Cenozoic extensional relics of Mesozoic compression. Geology 12, 550–554.

Cowgill, E., Yin, A., Harrison, T.M., Wang, X.F., 2003. Reconstruction of the Altyn Tagh fault based on U–Pb ion microprobe geochronology: role of back thrusts, mantle sutures, and heterogeneous crustal strength in forming the Tibetan Plateau. Journal of Geophysical Research 108, 2346.

Cui, J.W., 2011. Ductile shearing age of the south Altun fault and its tectonic implications. Acta Petrologica Sinica 27 (11), 3422–3434 (in Chinese with English abstract).

Cui, M.H., Meng, F.C., Wu, X.K., 2011. Early Ordovician island arc of Qimantag Mountain, eastern Kunlun: evidences from geochemistry, Sm–Nd isotope and geochronology of intermediate–basic igneous rocks. Acta Petrologica Sinica 27 (11), 3365–3379 (in Chinese with English abstract).

Davies, J.H., von Blankenburg, F., 1995. Slab breakoff: a model of lithosphere detachment and its test in the magmatism and deformation of collisional orogens. Earth and Planetary Science Letters 129, 85–102.

Dewey, J.F., 1988. Extensional collapse of orogens. Tectonics 7, 1123–1139.

Dewey, J.F., Bird, J.M., 1970. Mountain belts and the new global tectonics. Journal of Geophysical Research 75, 2625–2647.

Dixon, T.H., Batiza, R., 1979. Petrology and chemistry of recent lavas in the northern Marianas: implications for the origin of island arc basalts. Contributions to Mineralogy and Petrology 70, 167–181.

Dong, Z.C., Xiao, P.X., Xi, R.G., Guo, L., Gao, X.F., 2011. Geochemical characteristics and isotopic dating of bojites in the tectonic melange belt on south margin of Altun. Geological Review 57 (2), 207–216 (in Chinese with English abstract).

Dostal, J., Chatterjee, A.K., 2000. Contrasting behaviour of Nb/Ta and Zr/Hf ratios in a peraluminous granitic pluton Nova Scotia, Canada. Chemistry Geology 163, 207–218.

England, P., 1993. Convective removal of thermal boundary layer of thickened continental lithosphere: a brief summary of causes and consequences with special reference to the Cenozoic tectonics of the Tibetan Plateau and surrounding regions. Tectonophysics 223, 67–73.

Feng, C.Y., Li, C.Y., Li, G.C., Li, D.X., Zhou, A.S., Li, H.M., 2013. Ore-controlling structure and $^{40}Ar/^{39}Ar$ geochronology of Kekekaerde tungsten-tin deposit in Qimantage area, Xinjiang. Mineral Deposits 32 (1), 207–216 (in Chinese with English abstract).

Frey, F.A., Green, D.H., Roy, S.D., 1978. Integrated models of basalt petrogenesis: a study of quartz tholeiites to olivine melilitites from SE Australia utilizing geochemical and experimental petrological data. Journal of Petrology 19, 463–513.

Frisch, W., Kuhlemann, I.D.J., 2000. Post-collisional orogen-parallel large-scale extension in the Eastern Alps. Tectonophysics 327, 239–265.

Gao, Y.B., Li, W.Y., 2011. Petrogenesis of granites containing tungsten and tin ores in the Baiganhu deposit, Qimantage, NW China: constraints from petrology, chronology and geochemistry. Geochimica 40 (4), 324–336 (in Chinese with English abstract).

Guo, Z.F., Wilson, M., Liu, J.Q., Mao, Q., 2006. Post-collisional, potassic and ultrapotassic magmatism of the northern Tibetan Plateau: constraints on characteristics of the mantle source, geodynamic setting and uplift mechanisms. Journal of Petrology 47, 1177–1220.

Guo, T.Z., Liu, R., Chen, F.B., Bai, X.D., Li, H.G., 2011. LA-MC-ICPMS zircon U–Pb dating of Wulanwuzhuer porphyritic syenite granite in the Qimantag Mountain of Qinghai and its geological significance. Geological Bulletin of China 30 (8), 1203–1211 (in Chinese with English abstract).

Halliday, A.N., Mahood, G.A., Holden, P., Metz, J.M., Dempster, T.J., Davidson, J.P., 1989. Evidence for long residence times of rhyolitic magma in the Long Valley magmatic system: the isotope record in precaldera lavas of Glass Mountain. Earth and Planetary Science Letters 94, 274–290.

Harris, N.B.W., Inger, S., 1992. Trace element modeling of pelite-derived granites. Contributions to Mineralogy and Petrology 110, 46–56.

Hibbard, M.J., 1991. Textural anatomy of twelve magma-mixed granitoid systems. In: Didier, J., Barbarin, B. (Eds.), Enclaves and Granite Petrology. Dev Petrol, 13. Elsevier, Amsterdam, pp. 431–444.

Hoskin, P.W.O., 2000. Patterns of chaos: fractal statistics and the oscillatory chemistry of zircon. Geochimica et Cosmochimica Acta 64, 1905–1923.

Houseman, G.A., McKenzie, D.P., Molnar, P., 1981. Convective instability of a thickened boundary layer and its relevance for the thermal evolution of continental convergent belts. Journal of Geophysical Research 86, 6115–6132.

Jiang, C.F., Yang, J.S., Feng, B.G., Zhu, Z.Z., Zhao, M., Chai, Y., Shi, X.D., Wang, H.D., Hu, J.Q., 1992. Opening–Closing Tectonics of Kunlun Mountains. Geological Publishing House, Beijing, pp. 1–224 (in Chinese with English abstract).

Jung, S., Pfänder, J.A., 2007. Source composition and melting temperatures of orogenic granitoids: constraints from $CaO/Na_2O$, $Al_2O_3/TiO_2$ and accessory mineral saturation thermometry. European Journal of Mineralogy 19, 859–870.

Kay, R.W., Kay, S.M., 1993. Delamination and delamination magmatism. Tectonophysics 219, 177–189.

Krystopowicz, N.J., Currie, C.A., 2013. Crustal eclogitization and lithosphere delamination in orogens. Earth and Planetary Science Letters 361, 195–207.

Le Maitre, R.W. (Ed.), 1989. A Classification of Igneous Rocks and Glossary of Terms. Blackwell, Oxford (193 pp.).

Li, H.K., Lu, S.N., Xiang, Z.Q., Zhou, H.Y., Guo, H., Song, B., Zheng, J.K., Gu, Y., 2006. SHRIMP U–Pb zircon age of the granulite from the Qingshuiquan area, Central Eastern Kunlun Suture Zone. Earth Science Frontiers 13, 311–321 (in Chinese with English abstract).

Li, X.M., Ma, Z.P., Sun, J.M., Xu, X.Y., Lei, Y.X., Wang, L.S., Duan, X.X., 2009. Characteristics and age study about the Yuemakeqi mafic-ultramagic rock in the southern Altyn Fault. Acta Petrologica Sinica 25, 862–872 (in Chinese with English abstract).

Li, G.C., Feng, C.Y., Wang, R.J., Ma, S.C., Li, H.M., Zhou, A.S., 2012. SIMS zircon U–Pb age, petrochemistry and tectonic implications of granitoids in Northeastern Baiganhue W-Sn Orefield, Xinjiang. Acta Geoscientia Sinica 33 (2), 216–226 (in Chinese with English abstract).

Li, W., Neubauer, F., Liu, Y., Genser, J., Ren, S., Han, G., Liang, C., 2013. Paleozoic evolution of the Qimantagh magmatic arcs, Eastern Kunlun Mountains: constraints from zircon dating of granitoids and modern river sands. Journal of Asian Earth Sciences 77, 183–202.

Liégeois, J.P., 1998. Preface — some words on the post-collisional magmatism. Lithos 45, xv–xvii.

Liégeois, J.P., Navez, J., Hertogen, J., Black, R, 1998. Contrasting origin of post-collisional high-K calc-alkaline and shoshonitic versus alkaline and peralkaline granitoids. The use of sliding normalization. Lithos 45, 1–28.

Liu, L., Che, Z.C., Luo, J.H., Wang, Y., Gao, Z.J., 1996. Recognition and implication of eclogite in the western Altun Mountains, Xinjiang. Chinese Science Bulletin 42, 931–934 (in Chinese).

Liu, L., Che, Z.C., Wang, Y., Luo, J.H., Wang, J.Q., Gao, Z.J., 1998. The evidence of Sm–Nd isochron age for the early Paleozoic ophiolite in Mangya area, Altun Mountains. Chinese Science Bulletin 43, 754–756.

Liu, L., Sun, Y., Xiao, P.X., Che, Z.C., Luo, J.H., Chen, D.L., Wang, Y., Zhang, A.D., Chen, L., 2002. Discovery of ultrahighpressure magnesite-bearing garnet lherzolite (>3.8 GPa) in the Altyn Tagh, Northwest China. Chinese Science Bulletin 47, 881–886.

Liu, L., Sun, Y., Luo, J.H., Wang, Y., Chen, D.L., Zhang, A.D., 2004. Ultra-high pressure metamorphism of granitic gneiss in the Yinggelisayi area, Altun Mountains, NW China. Science in China Series D: Earth Sciences 47, 338–346.
Liu, L., Chen, D.L., Zhang, A.D., Sun, Y., Wang, Y., Yang, J.X., Luo, J.H., 2005. Ultrahigh pressure (>7 GPa) gneissic K-feldspar (-bearing) garnet clinopyroxenite in the Altyn Tagh, NW China: evidence from clinopyroxene exsolution in garnet. Science in China Series Series D: Earth Sciences 48, 1000–1010.
Liu, L., Zhang, J.F., Green, H.W., Jin, Z.M., Bozhilov, K.N., 2007. Evidence of former stishovite in metamorphosed sediments, implying subduction to >350 km. Earth and Planetary Science Letters 263, 180–191.
Liu, L., Wang, C., Chen, D.L., Zhang, A.D., Liou, J.G., 2009. Petrology and geochronology of HP–UHP rocks from the South Altyn Tagh, northwestern China. Journal of Asian Earth Sciences 35, 232–244.
Liu, L., Wang, C., Cao, Y.T., Chen, D.L., Kang, L., Yang, W.Q., Zhu, X.H., 2012. Geochronology of multi-stage metamorphic events: constraints on episodic zircon growth from the UHP eclogite in the South Altyn, NW China. Lithos 136–139, 10–26.
Liu, L., Cao, Y.T., Chen, D.L., Zhang, C.L., Yang, W.Q., Kang, L., Liao, X.Y., 2013. New progresses on the HP–UHP metamorphism in the South Altyn Tagh and the North Qinling. Chinese Science Bulletin 58, 2113–2123.
Lu, L., Wu, Z.H., Hu, D.G., Barosh, P.J., Hao, S., Zhou, C.J., 2010. Zircon U–Pb ages for rhyolite of the Maoniushan Formation and its tectonic significance in the East Kunlun Mountains. Acta Petrologica Sinica 26, 1150–1158 (in Chinese with English abstract).
Ludwig, K.R., 2003. Isoplot 3.0—a geochronological toolkit for Microsoft Excel. Berkeley Geochronology Center Spec Pub, pp. 1–70.
Ma, Z.P., Li, X.M., Xu, X.Y., Sun, J.M., Tang, Z., Du, T., 2011. Zircon LA-ICP-MS U–Pb isotopic dating for Qingshuiquan layered mafic–ultramafic intrusion southern Altun orogen, in northwestern China and its implication. Chinese Geology 38 (4), 1071–1078 (in Chinese with English abstract).
Maniar, P.D., Piccoli, P.M., 1989. Tectonic discrimination of granitoids. Geological Society of America Bulletin 101, 635–643.
Marotta, A.M., Ferna `ndez, M., Sabadini, R., 1998. Mantle unrooting in collisional settings. Tectonophysics 296, 31–46.
Miller, T.P., Chertkoff, D.G., Eichelberger, J.C., Coombs, M.L., 1999. Mount Dutton volcano, Alaska: Aleutian arc analog to Unzen volcano, Japan. Journal of Volcanology and Geothermal Research 89, 275–301.
Molnar, P., Tapponier, P., 1975. Cenozoic tectonics of Asia: effects of a continental collision. Science 189 (4201), 419–426.
Morrison, G.W., 1980. Characteristics and tectonic setting of the shoshonite rock association. Lithos 13, 97–108.
Murphy, J.B., 2013. Appinite suites: a record of the role of water in the genesis, transport, emplacement and crystallization of magma. Earth-Science Reviews 119, 35–59.
Oyhantçabal, P., Siegesmund, S., Wemmer, K., Frei, R., Layer, P., 2007. Post-collisional transition from calc-alkaline to alkaline magmatism during transcurrent deformation in the southernmost Dom Feliciano Belt (Braziliano-Pan-African, Uruguay). Lithos 98, 141–159.
Pan, Y.S., Zhou, W.M., Xu, R.H., Wang, D.A., Zhang, Y.Q., Xie, Y.W., Chen, T.E., Luo, H., 1996. Geological characteristics and evolution of the Kunlun Mountains region during the early Paleozoic. Science in China (Series D) 26, 302–307.
Patiño Douce, A.E., 1997. Generation of metaluminous a-type granites by low-pressure melting of calc-alkaline granitoids. Geology 25, 743–746.
Pearce, J.A., Baker, P.E., Harvey, P.K., Luff, I.W., 1995. Geochemical evidence for subduction fluxes, mantle melting and fractional crystallization beneath the South Sandwich Island arc. Journal of Petrology 36 (4), 1073–1109.
Peltzer, G., Tapponnier, P., 1988. Formation and evolution of strike-slip faults, rifts, and basins during the India–Asia collision: an experimental approach. Journal of Geophysical Research 93, 15085–15117.
Petford, N., Atherton, M., 1996. Na-rich partial melts from newly underplated basaltic crust: the Cordillera Blanca batholith, Peru. Journal of Petrology 37, 1491–1521.
Platt, J.P., Vissers, R.L.M., 1989. Extensional collapse of thickened continental lithosphere: a working hypothesis for the Alboran Sea and Gibraltar arc. Geology 17, 540–543.
Qi, S.S., Deng, J.F., Ye, Z.F., Liu, R., Wang, G.L., 2013. LA-ICP-MS zircon U–Pb dating of Late Devonian diabase dike swarms in Qimantag area. Geological Bulletin of China 32 (9), 1385–1393 (in Chinese with English abstract).
Rapp, R.P., Watson, E.B., 1995. Dehydration melting of metabasalt at 8–32 kbar: implication for continental growth and crust-mantle recycling. Journal of Petrology 36, 891–932.
Rickwood, P.C., 1989. Boundary lines within petrologic diagrams which use oxides of major and minor elements. Lithos 22, 247–263.
Ritts, B.D., Biffi, U., 2000. Magnitude of post-Middle Jurassic (Bajocian) displacement on the central Altyn Tagh fault system, northwest China. Geological Society of America Bulletin 112 (1), 61–74.
Rudnick, R.L., Gao, S., 2003. The composition of the continental crust. In: Rudnick, R.L. (Ed.), The Crust. Treatise on Geochemistry. Elsevier, Oxford, pp. 1–64.
Sobel, E.R., Arnaud, N., 1999. A possible middle Paleozoic suture in the Altyn Tagh, NW China. Tectonics 18, 64–74.
Solano, J.M.S., Jackson, M.D., Sparks, R.S.J., Blundy, J.D., Annen, C., 2012. Melt segregation in deep crustal hot zones: a mechanism for chemical differentiation, crustal assimilation and the formation of evolved magmas. Journal of Petrology 53, 1999–2026.
Sun, S.S., McDonough, W.F., 1989. Chemical and isotopic systematics of oceanic basalts; implications for mantle composition and processes. In: Saunders, A.D., Norry, M.J. (Eds.), Magmatism in the Ocean Basins. Geological Society of London Special Publications, 42, pp. 313–345.
Sun, J.M., Ma, Z.P., Tang, Z., Li, X.M., 2012. The LA-ICP-MS zircon dating and tectonic significance of the Yumuquan magma mixing granite, southern Altyn Tagh. Acta Geologica Sinica 86, 247–257 (in Chinese with English abstract).
Sylvester, P.J., 1998. Post-collisional strongly peraluminous granites. Lithos 45, 29–44.
Taylor, S.R., McLennan, S.M., 1995. The geochemical evolution of the continental crust. Review in Geophysics 33, 241–265.
Turner, S., 1992. Some geodynamic and compositional constraints on "postorogenic" magmatism. Geology 20, 931–934.
Turner, S.P., Platt, J.P., George, R.M.M., Kelley, S.P., Pearson, D.G., Nowell, G.M., April, R., Typescript, R., January, A., 1999. Magmatism associated with orogenic collapse of the Betic–Alboran Domain, SE Spain. Journal of Petrology 40, 1011–1036.
Vanderhaeghe, O., Teyssier, C., 2001. Partial melting and flow of orogens. Tectonophysics 342, 451–472.
Waight, T.M., Maas, R., Nicholls, I.A., 2001. Geochemical investigations of microgranitoid enclaves in the S-type Cowra Granodiorite, Lachlan Fold Belt, SE Australia. Lithos 56, 165–186.
Wang, Y., Liu, L., Che, Z.C., Chen, D.L., Luo, J.H., 1999. Geochemical characteristics of early Paleozoic ophiolite in Mangnai area, Alyun Mountains. Geological Review 45, 1010–1014 (Suppl., in Chinese with English abstract).
Wang, C., Liu, L., Luo, J., Che, Z., Teng, Z., Cao, X., Zhang, J., 2007. Late Paleozoic post-collisional magmatism in the Southwestern Tianshan orogenic belt: an example from the Baleigong pluton in the Kokshal region. Acta Petrlogica Sinica 23, 1830–1840 (in Chinese with English abstract).
Wang, C., Liu, L., Zhang, A.D., Yang, W.Q., Cao, Y.T., 2008. Geochemistry and petrography of Early Paleozoic Yusupuleke Tagh rapakivi-textured granite complex, South Altyn — an example for magma mixing. Acta Petrologica Sinica 24, 2809–2819 (in Chinese with English abstract).
Wang, X.L., Gao, X.P., Liu, Y.Q., Li, X.L., Zhou, X.K., et al., 2010. Revision of the Qimantagh Group in west part of East Kunlun. Northwestern Geology 43, 168–178 (in Chinese with English abstract).
Wang, C., Liu, L., Chen, D.L., Cao, Y.T., 2011. Petrology, geochemistry, geochronology and metamorphic evolution of garnet peridotites from South Altyn Tagh UHP terrane, NW China: records related to crustal slab subduction and exhumation history. In: Dobrzhinetskaya, L., Faryad, W., Wallis, S., Cuthbert, S. (Eds.), Ultrahigh Pressure Metamorphism: 25 Years After the Discovery of Metamorphic Coesite and Diamond. Elsevier, pp. 541–576.
Wang, B.Z., Luo, Z.H., Pan, T., Song, T.Z., Xiao, P.X., Zhang, Z.Q., 2012. Petrotectonic assemblages and LA-ICP-MS zircon U–Pb age of Early Paleozoic volcanic rocks in Qimantagh area, Tibetan Plateau. Geological Bulletin of China 31, 860–874 (in Chinese with English abstract).
Wang, C., Liu, L., Yang, W.Q., Zhu, X.H., Cao, Y.T., Kang, L., Chen, S.F., Li, R.S., He, S.P., 2013. Provenance and ages of the Altyn Complex in Altyn Tagh: implications for the early Neoproterozoic evolution of northwestern China. Precambrian Research 230, 193–208.
Watson, E.B., Harrison, T.M., 1983. Zircon saturation revisited temperature and composition effects in a variety of crustal magma types. Analysis 64, 295–304.
Whalen, J.B., Currie, K.L., Chappell, B.W., 1987. A-type granites: geochemical characteristics, discrimination and petrogenesis. Contributions to Mineralogy and Petrology 95, 407–419.
Whalen, J.B., Mcnicoll, V.J., Staal, C.R. Van, Lissenberg, C.J., Longstaffe, F.J., Jenner, G.A., Breeman, O. Van, 2006. Spatial, temporal and geochemical characteristics of Silurian collision-zone magmatism, Newfoundland Appalachians: an example of a rapidly evolving magmatic system related to slab break-off. Lithos 89, 377–404.
Williams, H.M., Turner, S.P., Pearce, J.A., Kelley, S.P., Harris, N.B.W., 2004. Nature of the source regions for post-collisional, potassic magmatism in southern and northern Tibet from geochemical variations and inverse trace element modelling. Journal of Petrology 45, 555–607.
Wilson, M., 1989. Igneous Petrogenesis—A Global Tectonic Approach. Alden Press, Oxford, (466 pp.).
Wu, G.J., Xiao, X.C., Li, T.D., 1989. The Yadong-Golmud geoscience section on the Qinghai–Tibet Plateau. Acta Geologica Sinica 63, 285–296 (in Chinese with English abstract).
Wu, S.P., Wu, C.L., Chen, Q.L., 2007. Characteristics and tectonic setting of the Tula aluminous A-type granite at the south side of the Altyn Tagh fault, NW China. Geological Bulletin of China 26 (10), 1385–1392 (in Chinese with English abstract).
XACGS, 2003. Geological Map of the Suwushijie, Xinjiang China, Scale 1: 250,000. Xi'an Center of Geological Survey, China Geological Survey (in Chinese).
Xu, Z.Q., Yang, J.S., Zhang, J.X., Jiang, M., Li, H.B., Cui, J.W., 1999. A comparison between the tectonic units on the two sides of the Altyn sinistral strike-slip fault and the mechanism of lithospheric shearing. Acta Geologica Sinica 73, 193–205 (in Chinese with English abstract).
Xu, Z.Q., Yang, J.S., Li, H.B., Yao, J.X., 2006. The Early Paleozoic terrane framework and the formation of the high-pressure (HP) and ultra-high pressure (UHP) metamorphic belts at the Central Orogenic Belt (COB). Acta Geologica Sinica 80, 1793–1806 (in Chinese with English abstract).
Xu, Z.Q., Yang, J.S., Li, H.B., Zhang, J.X., Wu, C.L., 2007. Orogenic Plateau: Terrane Amalgamation, Collision and Uplift in the Qinghai–Tibet Plateau. Geological Publishing House, Beijing, pp. 1–458 (in Chinese).
Yang, J.S., Liu, F.L., Wu, C.L., Wan, Y.S., Zhang, J.X., Shi, R.D., Chen, S.Y., 2003. Two ultrahigh pressure metamorphic events recognized in the central orogenic belt of China: evidence from the U–Pb dating of coesite-bearing zircons. Acta Geologica Sinica 77, 463–477 (in Chinese with English abstract).
Yang, W.Q., Liu, L., Ding, H.B., Xiao, P.X., Cao, Y.T., Kang, L., 2012. Geochemistry, geochronology and zircon Hf isotopes of the Dimunalike granite in South Altyn Tagh and its geological significance. Acta Petrologica Sinica 28, 4139–4150 (in Chinese with English abstract).
Yin, A., Harrison, T.M., 2000. Geologic evolution of the Himalayan–Tibetan Orogen. Annual Review of Earth and Planetary Sciences 28, 211–280.
Yin, A., Rumelhart, P.E., Butler, R., Cowgill, E., Harrison, T.M., Foster, D.A., Ingersoll, R.V., Zhang, Q., Zhou, X.Q., Wang, X.F., Hanson, A., Raza, A., 2002. Tectonic history of the

Altyn Tagh fault system in northern Tibet inferred from Cenozoic sedimentation. Geological Society of America Bulletin 114 (10), 1257–1295.
Yuan, H.L., Gao, S., Dai, M.N., Zong, C.L., Günther, D., Fontaine, G.H., Liu, X.M., DiWu, C.R., 2008. Simultaneous determinations of U–Pb age, Hf isotopes and trace element compositions of zircon by excimer laser ablation quadrupole and multiple collector ICP-MS. Chemical Geology 247, 100–118.
Zhang, J.X., Zhang, Z.M., Xu, Z.Q., Yang, J.S., Cui, J.W., 1999. The ages of U–Pb and Sm–Nd for eclogite from the western segment of Altyn Tagh tectonic belt. Chinese Science Bulletin 44, 2256–2259.
Zhang, J.X., Zhang, Z.M., Xu, Z.Q., Yang, J.S., Cui, J.W., 2001. Petrology and geochronology of eclogites from the western segment of the Altyn Tagh, northwestern China. Lithos 56, 187–206.
Zhang, J.X., Yang, J.S., Xu, Z.Q., Meng, F.C., Li, H.K., Shi, R.D., 2002. Evidence for UHP metamorphism of eclogites from the Altun Mountains. Chinese Science Bulletin 47, 751–755.
Zhang, A.D., Liu, L., Sun, Y., 2004. SHRIMP U–Pb zircon ages for the UHP metamorphosed granitoid gneiss in Altyn Tagh and their geological significance. Chinese Science Bulletin 49, 2527–2532.
Zhang, J.X., Mattinson, C., Meng, F.C., Wan, Y.S., 2005. An Early Palaeozoic HP/HT granulite–garnet peridotite association in the south Altyn Tagh, NW China: P–T history and U–Pb geochronology. Journal of Metamorphic Geology 23, 491–510.
Zhang, J.X., Meng, F.C., Yu, S.Y., 2010. Two contrasting HP/LT and UHP metamorphic belts: constraint on Early Paleozoic orogeny in Qilian–Altun orogen. Acta Petrologica Sinica 26 (7), 1967–1992 (in Chinese with English abstract).